村松久史　学位申請論文

主論文

Dissociation Rates of Oxygen and Ozone Molecules in the Stratosphere and the Mesosphere

H. Muramatsu

Meteorological Research Institute

Contents

Abstract

Photodissociation rates of oxygen and ozone molecules in the stratosphere, mesosphere and lower thermosphere were examined to see the uncertainties in treatment of the predissociation of the Schumann-Runge bands, the solar radiation and the transmission in the Schumann-Runge bands. And the effect of these uncertainties on the calculated distribution of the ozone molecule was estimated. First, we reviewed the previous studies about the predissociation of the Schumann-Runge bands. It is concluded that the vibrational levels of $B^3\Sigma_u^-$ state are predissociated to some extent between v'=3 and v'=17. This is confirmed by the spectroscopic and photochemical evidences, but questions remain about the repulsive states which cause the predissociation, relative importance of the underlying continuum, and the quantum yield of the ozone formation. Next, we reviewed the estimations of the solar ultraviolet radiation outside the atmosphere. Large variations or errors are caused by the followings: The first is the absolute intensity calibration. The second is the difference of the detectors. The third problem is the variability of the solar radiation.

We applied the band model to the calculations of the transmission in the Schumann-Runge bands. Examining the line broadening effects and line parameters we came to the conclusion that the random model for the inverse first power or the exponential distribution of line intensities with Lorentz line shape is most appropriate.

The remarkable contribution of the predissociation to the dissociation rate of the oxygen molecule appears above 45km. The maximum contribution appers at 75km for secz=1.0, at 80 km for secz=3.0 and at 85 km for secz=6.0. The ratio of the dissociation rate including the predissociation to that neglecting the predissociation falls in the range from 8 to 3.

Taking account of the uncertainty in the solar ultraviolet radiation due to the difference between the values obtained by the photographic technique and those by the photoelectric technique, the uncertainty of the factor 2 to 4 appears in the

dissociation rate of the oxygen molecule between 40 and 100 km.

The deviations of the dissociation rate of the oxygen molecule due to the various causes in the band model for the Schumann-Runge bands were estimated. The deviation due to the distribution functions (inverse first power distribution and exponential distribution) is at most 11 % between 40 and 100 km. The deviations due to the band model parameters are as follows: (1) 20 % due to the mean line intensity, (2) 20 % due to the mean line spacing, and (3) 5 % due to the mean line half-width.

The photodissociation rate of the ozone molecule is little affected by the predissociation or by the band model for the Schumann-Runge bands, but has the uncertainty of about 6 % between 40 and 100 km due to the ambiguity of the solar radiation. Vertical distributions of the ozone molecule in a pure oxygen atmosphere were calculated for the various combinations of the parameters. It is said that the profile deduced from the lower intensity of the solar radiation (obtained by the photoelectric technique) neglecting the predissociation of the oxygen molecule in the Schumann-Runge bands gives the better fit with the observed profiles than from other combinations of parameters, but the great discrepancy appears above 65 km. This discrepancy cannot be explained by the uncertainties that were discussed in this paper.

1. Introduction

The classical theories of ozone photochemistry in the atmosphere involving only oxygen reactions show higher ozone concentration than is observed (Hunt, 1966a). To solve this problem, Hunt(1966b) introduced the reactions involving hydrogen compounds in the photochemical reaction scheme. He showed that a satisfactory ozone profile can be obtained if the rate constants are taken properly. Hesstvedt(1968a,b) evaluated the effect of the vertical eddy transport and showed that the ozone distribution is affected by eddy motion below the height of 25 km and above 70 km. Crutzen(1970) pointed out the importance of NO and NO_2 in controlling the ozone concentrations in the stratosphere.

The photochemistry of the hydrogen and nitrogen oxides in the atmosphere involves many points still unclear : reaction scheme,rate constants, photodissociation rates, dissociation products and so on. Many of the species that appear in the reaction scheme have not been clearly observed in the upper atmosphere and the knowledge of the vertical eddy diffusion coefficients is poor. In this paper we discuss the effects of various uncertainties on the calculated photodissociation rate of oxygen and ozone molecules and determine the relative importance to the calculated ozone profile. This discussion would make the foundation of the ozone photochemistry both in a pure oxygen atmosphere and in an oxygen-hydrogen-nitrogen atmosphere.

Light absorption by the molecular oxygen has been observed from the near infrared to the far ultraviolet. Absorption shorter than 2500 Å is most important in the photochemical reactions of oxygen with some other molecules. For the formation of ozone in the atmosphere the absorption in the Herzberg continuum, the Schumann-Runge bands and the Schumann-Runge continuum is of primary interest. In the calculation of the dissociation rate of oxygen molecule in the wavelength region of the Schumann-Runge bands (1750-2050 Å) the principal sources of the uncertainties arise from predissociation, solar radiation and absorption cross section (or transmission).

Vibrationally excited levels of $B^3\Sigma_u^-$ state of oxygen molecule are known to be predissociated by absorption of light in the Schumann-Runge bands. This predissociation is confirmed by the spectroscopic evidences, but questions remain about the quantum yields of the photodissociation of oxygen molecule and the production of ozone molecule. We examine these problems from the reports up to date and study the effects of this predissociation to the aeronomy.

Next we examine the reported data of the solar ultraviolet radiation from the view-point of the absolute intensity calibration, observational techniques and the variability of the solar radiation, and study the effects of the variations of the solar intensity to the dissociation rate of the oxygen molecule.

There are several methods for the calculations of the atmospheric transmission in the Schumann-Runge bands. Because of the rapid variation of the absorption cross section and the overlapping of the lines, the method of the averaged cross section assuming the Lambert-Beer's law produces inaccuracies. The method of line-by-line calculations is more accurate but too tedious. Hudson and Mahle(1972) have carried out such a calculation. Fang et al.(1974) have calculated the photodissociation rates of several constituents by the application of opacity distribution functions to the transmission in the Schumann-Runge bands. There are ambiguities in the construction of the opacity distribution functions. The use of random selection of frequencies in each interval shows the slow convergency and so many points for each frequency interval are needed to ensure the accuracy. Park(1974) approximated the photodissociation rates of O_2, H_2O and NO using the equivalent exponential mean and pre-exponential mean absorption cross sections as a function of O_2 column density. These quantities are defined as functions of O_2 column density but are not expressed by a convenient form for the application.

In the present paper we attempted to apply a band model to the calculations of the transmission in the Schumann-Runge bands. The random model of the bands does not require the strict values of individual intensity, the line width and line position, but we need only the knowledge of the mean line intensity, mean line width, mean line spacing and the distribution of the line intensities. A preliminary

discussion of this random model in the Schumann-Runge bands has been made by Muramatsu et al. (1971), where the line parameters had not been known well. Using the newly obtained line parameters we discuss the validity of the band model in detail and deduce the uncertainties due to the model and the line parameters.

2. Predissociation in the Schumann-Runge bands

Absorption in the Schumann-Runge bands from 1750-2050 Å causes excitation to one of the vibrational levels of the $O_2(^3\Sigma_u^-)$ state. This state crosses the energy curves for the repulsive states and allows the predissociation of the excited molecule to ground-state oxygen atoms. Therefore the following reaction sequence is likely to occur:

$$O_2(^3\Sigma_g^-) + h\nu \longrightarrow O_2(^3\Sigma_u^-) \longrightarrow O_2^* \longrightarrow 2O(^3P)$$

where O_2^* is the oxygen molecule of the repulsive state. The photochemical and spectroscopic evidences thus far obtained support the predissociation, but there is some difference of opinion among the investigators as follows.

It was first suggested by Flory (1936) that the $^3\Sigma_u^-$ state is crossed by a $^3\Pi_u$ state as shown in Fig.1(a) at about v'=2. Here v' is the vibrational quantum number of $^3\Sigma_u^-$ state. His suggestion was based upon the fact that a weak fluorescence is observed at high oxygen pressure using 1849 Å excitation, while the fluorescence disappeared at low pressure. Further, he was unable to observe any emission from the $^3\Sigma_u^-$ state for v'> 2.

Volman(1956 a,b) has carried out photochemical experiments on the effect of foreign gases (O_2,N_2,A,He) on the rate of the formation of ozone by absorption of the Hg 1849 Å. He concluded that direct formation of atoms by a predissociation process proposed by Flory (1936) is most probable.

Wilkinson and Mulliken (1957) concluded from the rotational line broadening that predissociation of $^3\Sigma_u^-$ state takes place in the v'=12 level, and that it is probable from v'=4 to v'=11. Considering the possible states which can arise from neutral atoms, together with the selection rules for predissociation and correlation rules, they suggested that only $^3\Pi_u$ can predissociate $^3\Sigma_u^-$ strongly. They further suggested that $^3\Pi_u$ state predissociates the $^3\Sigma_u^-$ state at v'=12 on the left-hand side of the minimum of $^3\Sigma_u^-$ curve, and that this could explain the probable predissociation in all levels from v'=4 to v'=12, Fig.1(a). They also mentioned the possibility of a forbidden predissociation of the $^3\Sigma_u^-$ state

at $v'=3\frac{1}{2}$ by any of the $^5\Sigma_u^-$, $^1\Pi_u$ or $^5\Pi_u$ states. This forbidden predissociation would occur on the right-hand side of the minimum of the $^3\Sigma_u^-$ curve.

Carroll(1959) showed spectroscopically that predissociation is most pronounced for $v'=4$ passing through a minimum at $v'=9$ and rising to a secondary maximum at $v'=11$. He has suggested three possibilities:

(1) The unstable $^3\Pi_u$ state intersects the left limb of the $B^3\Sigma_u^-$ state between $v'=3$ and $v'=4$ (curve I, Fig.1(b)). In this case strong predissociation would be expected at $v'=4$, while higher vibrational levels also be predissociated.

(2) $A^3\Pi_u$ curve intersects $^3\Sigma_u^-$ on the right limb at about $v'=4$ (curve II, Fig.1(b)). It is possible that a quantum-mechanical treatment of the Franck-Condon principle might show that overlap integrals for $^3\Pi_u$ and $^3\Sigma_u^-$ state might pass through a minimum at $v'=9$ and show a subsidiary maximum at $v'=11$.

(3) It is possible that the predissociation at $v'\sim 11$ is caused by one of the other repulsive states ($^1\Pi_u$, $^5\Sigma_u^-$ or $^5\Pi_u$) which can arise from the configuration $^3P + ^3P$ (curve III, Fig.1(b)). Such a predissociation would be forbidden and would be weaker than that at $v'=4$.

Vanderslice et al.(1960) obtained potential energy curves for O-O interaction from approximate quantum-mechanical calculations. Using the crossing point at $v'=12$ of $B^3\Sigma_u^-$ state given by Wilkinson and Mulliken(1957), together with their values for the $^3\Pi_u$ curve at large distances, the equation for the $^3\Pi_u$ state was developed (Fig.1(c)). Their curve crosses the $^3\Sigma_u^-$ curve at the minimum, suggesting that predissociation should occur for the vibrational levels between 0 and 4. Further, their results indicate that the $^5\Sigma_u^-$ curve crosses the $B^3\Sigma_u^-$ curve right at $v'=3\frac{1}{2}$, supporting the suggestion of Wilkinson and Mulliken (1957).

Hudson and Carter (1968) found from the measurements on the Schumann-Runge system at elevated temperature that the all of the vibrational levels of the $B^3\Sigma_u^-$ state from $v'=3$ to 17 are subject to predissociation, suggesting that

the intersection of $^3\Pi_u$ and $B^3\Sigma_u^-$ states occurs between v'=2 and v'=3. They found that the smallest predissociation line width was 0.3 cm^{-1}, and that at least 99 % of the oxygen molecules that are excited into the $B^3\Sigma_u^-$ state for v'>2 will predissociate.

Schaefer and Harris (1968) have carried out the *ab initio* quantum mechanical calculations on the potential energy curves of molecular oxygen. The calculated $^3\Pi_u$ repulsive curve crosses the inner limb of the $B^3\Sigma_u^-$ curve. This is in agreement with the results of Wilkinson and Mulliken (1957) and to a lesser degree with those of Vanderslice et al. (1960). Their calculations also show that the repulsive states mentioned by Carroll (1959), $^1\Pi_u$, $^5\Sigma_u^-$ and $^5\Pi_u$ cross the $B^3\Sigma_u^-$ potential curve in such a way that they might give rise to forbidden predissociations (Fig.1(d)).

Murrell and Tayler (1969) have applied the Franck-Condon principle to predissociation in the Schumann-Runge bands of O_2. They have found that the best agreement with the observed strong and weak predissociations at v'=4 and v'=11 was obtained by a single repulsive curve which crosses the outer limb of the $B^3\Sigma_u^-$ near v'=4 but has no other crossing point. Their results did not support the calculations of Schaefer and Harris (1968), (Fig.1(e)).

Ackerman and Biaumé (1970) have photographed at high resolution the spectra of the Schumann-Runge bands from 0-0 to 13-0 bands. They point out that the variation of the apparent half-width as a function of the vibrational quantum number may by partly interpreted in terms of predissociation. The observed maximum at v'=4 may be caused by the predissociation, however the maximum at v'=7 and v'=11 may be partly due to the superposition. Their results appear to be in good qualitative agreement with the theoretical results obtained by Murrell and Taylor (1969). They concluded that their experimental data do not fully support the results of Murrell and Taylor (1969) and that another type of experimental measurement is required.

Ogawa (1971) has investigated absorption cross section on the underlying continuum of the Schumann-Runge bands and discussed the potential curve of the upper state of the dissociation continuum. He says that any part of the observed absorption cross section does not correspond to the $^3\Pi_u - X^3\Sigma_g^-$ transition if the $^3\Pi_u$ curve intersects the right limb of the $B^3\Sigma_u^-$ state between $v'=3$ and 4, because the Franck-Condon factor of such a $^3\Pi_u - X^3\Sigma_g^-$ transition would be rather small under such circumstances. He states further that if the potential curve of the $^3\Pi_u$ state intersects the left limb of the $B^3\Sigma_u^-$ state, it is possible that an appreciable part of the underlying Schumann-Runge continuum may be due to the $^3\Pi_u - X^3\Sigma_g^-$ transition.

Schaefer and Miller (1971) calculated *ab initio* potential curves for the $B^3\Sigma_u^-$, $^3\Pi_u$ and $^1\Pi_u$ state of a much higher reliability than those of Schaefer and Harris (1968). They concluded that $^3\Pi_u$ curve crosses the inner limb of the $B^3\Sigma_u^-$ state curve somewhat above $v'=4$, while the $^1\Pi_u$ curve crosses the outer limb between $v'=0$ and $v'=1$. They further state that spin-orbit coupling is the principal interaction responsible for the predissociation, so that all four repulsive states ($^1\Pi_u$, $^3\Pi_u$, $^5\Pi_u$, $^5\Sigma_u^-$) which dissociate to ground state atom are expected to predissociate $B^3\Sigma_u^-$ to roughly the same degree.

Wilkinson and Mulliken (1957) have pointed out that a direct transition from $^3\Sigma_g^-$ to $^3\Pi_u$ is possible and have observed a weak continuum associated with this transition. They suggested that this transition is more important in the decomposition of oxygen above 1750 Å. If this were the case, the quantum yield of ozone formation would have to be small at 1849 Å.

Washida et al. (1971) have obtained the quantum yield of ozone formation by decomposition of excited oxygen molecules at two wavelengths. The quantum yield of ozone formation was 2.0 at 1849 Å and 0.3 at 1931 Å. They state that their experimental results can be explained by direct transition from $X^3\Sigma_g^-$ to the repulsive $^3\Pi_u$ state at 1848.6 Å, and that the transition to the rather stable rotational level of $v'=4$ of $B^3\Sigma_u^-$ occurs at 1930.9 Å, where rotational level

can predissociate only within 15 %.

Most workers agree that all vibrational levels $v'=3$ to 17 are predissociated to some extent, and this could be caused primarily by the $^3\Pi_u$ state which intersects the potential curve of the $B^3\Sigma_u^-$. Several questions remain for the predissociation of the Schumann-Runge bands at present:

(1) Crossing point of $^3\Pi_u$ state with $B^3\Sigma_u^-$ state. It is not established whether $^3\Pi_u$ crosses on the inner branch or the outer branch of $B^3\Sigma_u^-$.

(2) The cause of the predissociation maxima seen at $v'=4$, 7 and 11. It is not clear whether it arises from repulsive states $^5\Pi_u$, $^5\Sigma_u^-$ and $^1\Pi_u$, or it arises from experimental difficulties as Ackerman and Biaumé (1970) state, or it arises from the interference effects in the Franck-Condon factor associated with a single crossing as Murrell and Taylor (1969) obtained.

(3) The contribution of the repulsive states $^5\Pi_u$, $^5\Sigma_u^-$ and $^1\Pi_u$ to the predissociation.

(4) The contribution and the relative importance of the underlying continuum to the dissociation.

(5) The quantum yield of the ozone formation by the decomposition of excited oxygen molecule in the Schumann-Runge system.

Because of the aforementioned questions, we suppose in the following calculations the two limited cases. In the first case we suppose that the oxygen molecules that are excited into the $B^3\Sigma_u^-$ state for $v' > 2$ would be completely predissociated. In the second case we suppose that the predissociation does not occur, while the oxygen molecules are dissociated by the underlying continuum.

3. Solar flux

The spectral region of the solar flux between 3000 Å and 1000 Å is important in the chemical and the thermal balance of the upper atmosphere. The solar flux between 2000 Å and 1300 Å is especially important because it dissociates molecular oxygen, supplying the main source of atomic oxygen and heat in the lower thermosphere, mesosphere and upper stratosphere. The large differences are recognized among the reported solar radiations between 1300 Å and 2000 Å. In Figure 2 some of the reported data are shown.

Curve (1) is the result of Johnson (1954) using the concave grating rocket-borne spectrograph down to 2200 Å.

Curve (2) is the solar spectrum given by Detwiler et al. (1961) by means of grating spectrographs below 2600 Å. The 1700 Å to 1520 Å spectral range was obtained by interpolation between the two sets of experimental data.

Widing et al. (1970) reported the result of ten solar rocket spectra photographed on July 27, 1966 between 2075 Å and 1450 Å. Their result is shown by the dashed curve (3). They state that their values are in good agreement with those of Bonnet (1968), which were obtained by rocket-borne spectrograph and by completely independent calibration. They also state that experimental error is of the order $\pm$ 30 % in the 1650 Å range. They say that if the separate sources of error act in the same direction in the calibration, the uncertainty in the calibration of the absolute intensity in the 1650 Å region would reach a factor of 1.6 or 1.8.

Brueckner and Moe (1972) measured the absolute intensities of the solar ultraviolet continuum from 1400 Å to 1790 Å from rocket spectra. Their measurement were in good agreement with the intensities of Widing et al. (1970).

Brewer and Wilson (1965) measured intensities of direct and scattered radiation in the 2100 Å window by means of balloon-borne platinum-cathode photocell. They found that the calculated intensity of solar radiation in the 2100 Å window only agrees with the measurements if the following two adjustments are made to the

data used. The oxygen absorption cross-section by Ditchburn and Young (1962) require to be multiplied by 0.75 and the solar intensity outside the atmosphere given by Detwiler et al. (1961) by 0.36. The dotted curve in Figure 2 between 2425 Å and 1800 Å is the complete adjusted data used to obtain the close agreement between the observed and calculated data. Their values are lower by a factor of 3 in the 1800 Å region and a factor of 2.8 in the 2000 Å region than the values of Detwiler et al. (1961).

In 1969, Parkinson and Reeves (1969) reported a new solar spectrum for the wavelength range 1400 Å - 1875 Å. It is shown by the curve (5) in Figure 2. Spectral intensities of the solar continuum were obtained from a rocket-borne photoelectric spectrometer. These intensities are lower than those of Widing et al. (1970) by a factor of 2 at 1875 Å and a factor of 3 at 1600 Å.

Prag and Morse (1970) have measured the solar flux in three broad wavelength intervals; 300-1150 Å, 1150-1600 Å and 1600-2100 Å with photodiodes from the satellite. Their data are consistent with a model in which the effective plage temperature is about 1250°K higher than the background sun at all wavelength intervals. The effective temperature of the background solar disk was 4440°K in the 1600-2100Å region. This effective temperature gives the solar intensity which agrees well with the data of Parkinson and Reeves (1969).

Heath (1973) observed the UV solar irradiance by photometers consisting of broad band sensors (combination of optical filters and photodiodes) from a rocket and satellites. The rocket observations of the solar irradiance (Aug.1966) are significantly lower in the vicinity of 1750 Å (by about a factor of 3) than NRL values (Widing et al. 1970) for a rocket flight about a month earlier. For wavelengths below 1800 Å, the solar irradiance observed from the satellites is consistent with the Harvard observation (i.e. Parkinson and Reeves,1969) and significantly lower than those reported by NRL (i.e. Widing et al. 1970).

Nishi et al. (1973) measured the absolute intensity of the sun at three wavelengths 1629 Å, 1684 Å and 1739 Å by the rocket-borne concave diffraction gratings and CsTe-cathode photomultiplier. Their results agree with those of Parkinson and Reeves (1969) and shown in Figure 2.

The dispersion of the observed solar spectral intensities below 2500 Å may be caused by the following several sources. First there is the technical problem of the absolute intensity calibration. There has been no absolute calibrated continuum light source to compare with in the extreme ultraviolet region. Detwiler et al. (1961) estimated that the accuracy is better than ± 20 % and there are no errors greater than a factor of ± 1.5 in the region 2000 Å to 1400 Å. Below 1300 Å they state there is the possibility of errors as great as a factor ± 2, and in places perhaps more.

Widing et al. (1970) state that main uncertainties are the error in the calibration of the carbon arc and its reproducibility and errors in the plate microphotometry. They estimate that the uncertainty in the arc stream at the short wave end (~1950 Å) might be as much as ± 20 % relative to those at the long wave end (2400 Å) and the variations in the arc are 3 to 4 %, and the microphotometry error might be 5 %. So the uncertainty in the continuum intensities in the 2000 Å region is of the order ± 30 %. In the 1650 Å region, they say that if the separate sources of the error act in the same direction the uncertainty in the calibration of the absolute intensity could reach a factor of 1.6 or 1.8.

Brueckner and Moe (1972) calibrated the instrument for the wavelength longer than 1660 Å by a deuterium lamp , the intensity of which has been measured against a known synchrotron source, and estimated the accuracy of the lamp calibration to be ± 15 %. Another check of the intensity of the lamp using a diode which was calibrated absolutely by the National Bureau of Standards, was done and the resulting intensities differed by less than 10 % from the synchrotron calibration values.

The second problem is the variability of the solar radiation. There are two

kinds of variation; the solar cycle variation and the spatial variation over the solar surface. As for the solar cycle variation, intensity variations in the visible region in time are very small, but in the extreme ultraviolet region considerable changes are observed.

Heath (1973) concluded from the data of satellites and rockets that there is a significant variation in the solar irradiance in the vicinity of 1750 Å, and this variation appears to follow the 11-year solar cycle. In Figure 3 variations of ultraviolet fluxes during a solar cycle are shown. Intensities of the 284 Å (Fe XV), the 630 Å (O V) and the 1025 Å (H I) emission lines are adopted from Hall et al. (1969). Hall et al. (1969) state that the errors of the observed values are about 20 % for most of the dates, and these errors tend to obscure somewhat the solar cycle variation. The 284 Å line and the 335 Å line (not shown in the Figure) have the clear variation but the other lines (304 Å, 584 Å, 625 Å, 630 Å, 977 Å, 1025 Å 1032 Å) show the same general shape, a depression in the period 1963-1965 and an increase by the end of 1968 to values exceeding their minimum levels by factors ranging from 1.5 to 2.3. In the uppermost part of the same Figure, are shown the Wolf's relative sun-spot number as the indicator of solar activity, and the solar intensity of the 1750 Å region. We cannot deduce any definite variation corresponding to the 11-year solar cycle for the solar intensity of 1750 Å region.

The variation of the incident extreme ultraviolet fluxes with solar rotation (27-day variation) is known and its amplitude is an order of magnitude comparable to that of 10.7 cm coronal emission according to Hinteregger (1970). Prag and Morse (1970) showed that solar flux varied more than 50 % from the mean in the two longer wavelength regions (1150-1600 Å, 1600-2100 Å) during the first 27 days. All three wavelength channels showed much stronger correlation with the area times intensity of calcium plage regions than the 10.7 cm radio flux. Heath (1973) observed the variations of solar irradiance associated with the solar rotational period from the satellite. The change in irradiance with solar rotation increased with decreasing wavelength and the magnitude of variation was smaller than that of Prag and Morse (1970).

It is mainly the radiation from the entire sun (or the solar irradiance) which is interested in the photochemistry of the earth's atmosphere but the some measurements are made for the special positions on the solar disk. The variations of the emissions over the solar disk are great in the extreme ultraviolet. Observations of the centre-to-limb variations of the intensity in the extreme ultraviolet are very few. Observations by Brueckner and Moe (1972) and Nishi et al. (1973) show that the intensity decreases from centre to limb at 1750 Å, 1739 Å and 1684 Å while below 1600 Å the intensity is remarkably neutral and increases in the extreme limb. The radiation from the solar active region is several times stronger than that from the quiet portions of the sun. Dupree et al. (1973) observed extreme ultraviolet radiation (280-1370 Å) of a solar active region and of the quiet solar atmosphere from OSO-6 satellite. Intensities from the active region is increased by almost one order of magnitude compared with those from the quiet region at the disk center.

We can recognize from the Figure 2 and Figure 3 that the solar intensities measured by the photographic technique adopted by the NRL group (the values of Johnson (1954), Detwiler et al.(1961), Widing et al. (1970) and Brueckner and Moe (1972), shown by filled circles in Figure 3) are all stronger than those by photoelectric technique (Brewer and Wilson (1965), Heath (1973), Prag and Morse (1970), Parkinson and Reeves (1969) and Nishi et al. (1973), shown by filled squares in Figure 3).

The photographic technique uses the photographic emulsions and as stated by Hudson (1971) they have the advantage of allowing the entire absorption spectrum to be recorded simultaneously but they have the disadvantages that the calibration is not simple and that the photographic density is not a linear function of the incident photon flux and there are other sources of error from the development procedures and others. The photoelectric technique uses the photoelectric detectors and has the advantage that the detectors have a linear response between their

output and the incident-photon flux over a wide range of values. As stated before the intensities measured by photoelectric technique are in general lower by a factor of 3 than those by photographic technique. This discrepancy has not yet been explained by any observers, while Hinteregger (1970) recommended that measurements by Parkinson and Reeves (1969) are more reliable and for the moment, we should use the values of Detwiler et al. (1961) reducing all fluxes of the 1300-1800 Å range by a common factor of 3.

It is seen from the above discussions that the largest source of the dispersion of the observed solar radiation is the difference of the detectors. For the aeronomical interest, we need the data on the spectral intensity distribution from the entire sun for various solar activities. The data available at the present are scanty and the discrepancies among the data are not settled yet, so we assumed the three solar intensity distributions in the following calculations. The adopted data are from the following sources:

Case A : $\lambda \geq 2600$ Å ; Johnson (1954)

$2600 \text{ Å} > \lambda \geq 1300$ Å ; Detwiler et al. (1961)

$1300 \text{ Å} > \lambda \geq 1000$ Å ; Hinteregger (1970)

Case B : $\lambda \geq 2600$ Å ; Johnson (1954)

$2600 \text{ Å} > \lambda \geq 2075$ Å ; Detwiler et al. (1961)

$2075 \text{ Å} > \lambda \geq 1450$ Å ; Widing et al. (1970)

$1450 \text{ Å} > \lambda \geq 1300$ Å ; Detwiler et al. (1961)

$1300 \text{ Å} > \lambda \geq 1000$ Å ; Hinteregger (1970)

Case C : $\lambda \geq 2425$ Å ; Johnson (1954)

$2425 \text{ Å} > \lambda \geq 2050$ Å ; Brewer and Wilson (1967)

$2050 \text{ Å} > \lambda \geq 1875$ Å ; Interpolation

$1875 \text{ Å} > \lambda \geq 1425$ Å ; Parkinson and Reeves (1969)

$1425 \text{ Å} > \lambda \geq 1300$ Å ; Interpolation

$1300 \text{ Å} > \lambda \geq 1000$ Å ; Hinteregger (1970)

Case A represents the old data of NRL group in the Schumann-Runge region. Case B represents the new data of NRL group by Widing et al. (1970), which shows lower intensities than the old data. Measurements of Case A and Case B, except that of Hinteregger (1970), were done by the photographic technique. The data of the Case C were adopted from measurements by the photoelectric technique and the intensities are lower by a factor of 3 or 2 than that of Case A in the main parts of the wavelength region which gives rise to the dissociation of the oxygen molecule. The solar intensities of Case A and Case C were assumed to be the critical values of the uncertainty in the observations. In the following calculations, we examine the the influences of the deviations of the solar intensity (i.e. Case A, Case B and Case C described above) on the dissociation rate of oxygen molecule and the formation of ozone molecules.

4. Random model approximation

Absorption cross sections of the Schumann-Runge bands vary between $10^{-19}cm^2$ (at 1750 Å) and $10^{-23}cm^2$ (at 2050 Å) , as shown in Figure 4, so the solar radiation penetrates to the bottom of the stratosphere and dissociates the oxygen molecule in the stratosphere and mesosphere. Each band is composed of many overlapping rotational lines as shown in Figure 5. Because of the rapid variation of the absorption cross section and the overlapping of the lines the method of the average band-absorption cross sections assuming the Lambert-Beer's law produces inaccuracy. In the present paper we discuss the application of the band model approximation for the transmission of the solar radiation in the Schumann-Runge bands.

Two models which are physically distinct for the spectral band absorption are known (Goody,1964). The first one is the Elsasser model. This model assumes that a band consists of an infinite number of spectral lines with the same intensity, half-width and spaced at equal intervals. The Elsasser model has been exactly solved only for the Loretz line shape. On the other hand the random model of a band assumes that the positions of the individual spectral lines occur at random and the intensities can be represented by the probability functions.

For the most part of the Schumann-Runge bands as shown in Figure 5, position of the spectral lines and intensities can be treated as occurring at random, so we approximate the absorption in the bands with a random model.

4.1 Line position

Neglecting the triplet splitting due to electron spins, the wave number ν of the rotational lines are determined from the relation

$$\nu = \nu_0(v',v'') + (B_{v'}+B_{v''})m + (B_{v'}-B_{v''}-D_{v'}+D_{v''})m^2 - 2(D_{v'}+D_{v''})m^3 - (D_{v'}-D_{v''})m^4 \qquad (1)$$

where primes indicate the upper vibrational state, and double primes the lower

vibrational state. $\nu_0(v',v'')$ is the band origin of the vibration-rotation band. $B_{v'}, D_{v'}, B_{v''}, D_{v''}$ are the rotational constants of the upper vibrational level v' and the lower vibrational level v''. m is an index number related to the rotational quantum number N, corresponding to the total angular momentum apart from spin, by

$m = -N$ for the P branch, and

$m = N + 1$ for the R branch.

$B_{v''}$ and $D_{v''}$ for the $X^3\Sigma_g^-$ state were calculated from

$$B_{v''} = B_e - \alpha_e(v'' + 1/2) \quad \text{and} \quad D_{v''} = D_e + \beta_e(v'' + 1/2)$$

and the data for B_e, α_e, D_e and β_e were taken from Herzberg (1950). Adopted values are

$B_{v''} = 1.437771\ cm^{-1}$, $D_{v''} = 4.913 \times 10^{-6} cm^{-1}$ for $v'' = 0$ and

$B_{v''} = 1.421979\ cm^{-1}$, $D_{v''} = 4.825 \times 10^{-6} cm^{-1}$ for $v'' = 1$.

Band origin $\nu_0(v',0)$ and rotational constants $B_{v'}, D_{v'}$ were taken from Ackerman and Biaume (1970) for v'=0-12 and from Brix and Herzberg (1954) for v'=13-20. $\nu_0(v',1)$ was calculated from the relation

$$\nu_0(v',1) = \nu_0(v',0) + G(v''=0) - G(v''=1)$$
$$= \nu_0(v',0) - 1556.393\ cm^{-1}$$

where $G(v'')$ is the vibrational term value for the $X^3\Sigma_g^-$ and adopted from Herzberg (1950). The values of the band origin and rotational constants are shown in Table 1.

4.2 Line shape

Several factors lead to the broadening of the spectral line. The magnitude of the line broadening is expressed in term of 'half-width' as shown in Figure 6. Often, 'half-width' is called 'half-intensity width' or 'full half-width'. These are the widths of the line at the intensity one-half of the maximum intensity of emission or absorption. One-half of the 'half-width' is called 'half half-width'.

Predissociation line widths for the Schumann-Runge system obtained by Ackerman et al. (1970) and Hudson and Mahle (1972) are shown in Table 2. Excepting those for $v'=0$ and $v'=1$ half-widths are between 0.06 and 3.70 cm^{-1}. According to Rice (1930), line shapes can be treated as the Lorentz profile for a resonance process such as predissociation. Other line-broadening effects that contribute to the line shape were examined.

(a) Natural broadening

If we assume the radiative lifetime to be 5.3×10^{-9} sec (Herzberg,1950), the natural line width (half-width) becomes 0.001 cm^{-1}.

(b) Doppler broadening

Doppler width increases as the square root of the temperature. The Doppler line widths are 0.102 cm^{-1}(200°K), 0.125 cm^{-1}(300°K) for 1750 Å and 0.089 cm^{-1} (200°K), 0.109 cm^{-1}(300°K) for 2000 Å. Thus Doppler line widths are smaller than the predissociation line widths except for $v'=13$ and 14. (Predissociation is not observed from $v'=0$ to 2)

(c) Pressure broadening

The line broadening by the elastic collision with another molecule is proportional to the pressure from the impact theory (Goody,1964). Collision line widths (half-widths) from the impact theory are 4.6×10^{-3} cm^{-1} at the altitude of 20 km, $2.2 \times 10^{-4} cm^{-1}$ at 40 km and $1.7 \times 10^{-5} cm^{-1}$ at 60 km.

It is concluded from the above discussion that the natural and pressure broadening are negligible compared with the predissociation broadening. The Doppler broadening can not be completely neglected for some bands, where the combined Lorentz and Doppler broadening should be considered. If we take the Lorentz and Doppler line widths into account, the line shape of the Schumann-Runge bands can be expressed by a Voigt profile, but in the following calculations we assume a Lorentz line shape for simplicity.

4.3 Random model for Lorentz line shape

According to the theory of the random model approximation, the mean transmission over a certain wave number region that contains enough spectral lines is given by (Goody, 1964)

$$\bar{T} = \exp(-\bar{W}_{s\ell} / \bar{d}) \qquad (2)$$

where $\bar{T}$ is the mean transmission, $\bar{d}$ is the mean line spacing, and $\bar{W}_{s\ell}$ is the mean of the equivalent width of the single line $W_{s\ell}$. The equivalent width of a single line is defined as

$$W_{s\ell} = \int \{1 - \exp(-bSa)\} d\nu$$

where ν is the wave number, S the total intensity of the line, a the amount of the absorbing gas per unit area and b the line shape factor normalized to unity,

$$\int_{-\infty}^{\infty} b(\nu) d\nu = 1.$$

The line shape factor for the Lorentz line is given by

$$b(\nu) = \frac{\alpha}{\Pi(\nu^2 + \alpha^2)}$$

where α is the half half-width of the line, and ν the deviation of wave number from the line center.

For the calculation of $\bar{W}_{s\ell}$, we must know the distribution of line intensities. Let $p(S)dS$ be the probability that a line has an intensity between S and $S + dS$. Then the $\bar{W}_{s\ell}$ is given by

$$\bar{W}_{s\ell} = \int_0^{\infty} W_{s\ell}\, p(S) dS.$$

For the lorentz line shape, $\bar{W}_{s\ell}$ is given by

$$\bar{W}_{s\ell} = \int_0^{\infty}\int_{-\infty}^{\infty} p(S)\left\{ 1 - \exp\left(- \frac{Sa\,\bar{\alpha}}{\Pi(\nu^2 + \bar{\alpha}^2)}\right)\right\} d\nu dS,$$

where $\bar{\alpha}$ is the mean half half-width of the line. The equivalent width for a line with the Lorentz line shape can be integrated exactly and given as (Goody,1964)

$$\bar{W}_{s\ell} = 2\Pi\bar{\alpha}\exp(-x)\ [\ I_0(x) + I_1(x)\ ],$$

where $x = Sa/2\Pi\bar{\alpha}$ and I_0 and I_1 are the Bessel functions of imaginary argument. Then the $\bar{W}_{s\ell}$ becomes.

$$\bar{W}_{s\ell} = 2\Pi\bar{\alpha}\int_0^{\infty} x\exp(-x)\ [\ I_0(x) + I_1(x)\ ]p(S)dS \qquad (3)$$

For the several kinds of the intensity distribution , $\bar{W}_{s\ell}$ can be calculated.

(a) Exponential distribution of line intensities.

The probability function is given by

$$p(S) = \bar{S}\ \exp(-\ S\ /\ \bar{S}\ ) \qquad (4)$$

where $\bar{S}$ is the mean line intensity. Then $\bar{W}_{s\ell}$ and $\bar{T}$ are given by

$$\bar{W}_{s\ell} = \frac{\bar{S}a}{\sqrt{1 + \bar{S}a/\Pi\bar{\alpha}}}$$

$$\bar{T} = \exp\left(- \frac{\bar{S}a/\ \bar{d}}{\sqrt{1 + \bar{S}a/\Pi\bar{\alpha}}}\right) \qquad (5)$$

(b) Inverse first power distribution.

The probability function is given by

$$p(S) = K\ /\ S\ ,\quad S \leq S_2 \qquad (6)$$

where K is constant. Then $\bar{W}_{s\ell}$ becomes

$$\bar{W}_{s\ell} = 2\Pi\bar{\alpha}K[\ 2u\left\{ I_0(u) + I_1(u)\right\}\exp(-u) + I_0(u)\cdot\exp(-u) - 1] \qquad (7)$$

where $u = S_2a/2\Pi\bar{\alpha}$.

(c) Constant probability distribution.

The probability function is given by

$$p(S) = K \qquad (8)$$

where K is constant. If we represent the maximum and minimum intensities as

S_2 and S_1 respectively, K is given by

$$K = 1 / (S_2 - S_1) .$$

In the limit $S_1 \rightarrow 0$, $\bar{W}_{S\ell}$ becomes

$$\bar{W}_{S\ell} = \frac{2\Pi\bar{\alpha}}{3u} [\, 2u^2 I_0(u)\cdot\exp(-u) + 2u^2 I_1(u) - uI_1(u)\cdot\exp(-u) \,]$$

where $u = S_2 a / 2\Pi\bar{\alpha}$.

(d) All of the spectral lines are equally intense.

The probability function is given by Dirac δ-function

$$p(S) = \delta(S - \bar{S}) . \qquad (9)$$

Then, $\bar{W}_{S\ell}$ is given by

$$\bar{W}_{S\ell} = 2\Pi\bar{\alpha}u \exp(-u) [\, I_0(u) + I_1(u) \,]$$

where $u = \bar{S}a/2\Pi\bar{\alpha}$.

For the application of the random model to the absorption of the Schumann-Runge bands, we must know the following parameters: (1) distribution function of line intensities (2) mean line half-width (3) mean line intensity (4) mean line spacing.

4.4 Integrated band absorption coefficient

The integrated band absorption coefficient $K(v',v'')$ (cm^{-2}) for v'-v'' band is defined as

$$K(v',v'') = \int_{\nu'_{v''}} k(\nu)d\nu$$

where $k(\nu)$ (cm^{-1}) is the absorption coefficient contributed by the vibrational transition $v'' \rightarrow v'$. Integrated band absorption coefficient is also expressed by the total band absorption oscillator strength, $f(v',v'')$, following Herzberg(1950) and Bethke (1959a) as

$$K(v',v'') = \frac{N_L \Pi e^2}{m c^2} f(v',v'') F(v'') = 2.379 \times 10^7 f(v',v'') F(v'') \qquad (10)$$

where c is the velocity of light, N_m the number of molecules cm^{-3} at 1 atm and 0°C and m and e the mass and the charge of the electron, respectively. F(v") is the fraction of molecule in the lower vibrational state. The total band absorption oscillator strength f(v',v") can be expressed by the Franck-Condon factor (the overlap integral squared), q(v',v"), and the electronic absorption oscillator strength, f_{el} , by the relation (Bethke, 1959a).

$$f(v',v'') = f_{el}\, q(v',v'')\, \nu_0(v',v'')/\bar{\nu} \quad . \qquad (11)$$

Here $\bar{\nu}$ is the q(v',v") weighted average wave number of the transition, and $\nu_0(v',v'')$ is the wave number of the band origin. We adopted the value of $\bar{\nu}$ from Bethke (1959b), i.e. 68380 cm^{-1}, which is nearly the wavenumber at the maximum absorption in the Schumann-Runge continuum. The value of f_{el} was adopted from Bethke (1959b), which is equal to 0.163.

In the v"=0 progression, integrated band absorption coefficients have been measured by Ditchburn and Heddle (1954), Bethke (1959b), Halmann (1966), and Farmer et al. (1968). Theoretically calculated values for the Franck-Condon factors are reported by Jarmain (1963), Ory and Gittleman (1964), Halmann and Laulicht (1966), Murrell and Taylor (1969), Harris et al. (1969) and Allison et al. (1971). From these Franck-Condon factors, integrated band absorption coefficients can be calculated by the Equations (10) and (11). Experimental and theoretical values of K(v',v") for v"=0 are shown in Figure 7. Experimentally obtained values of Bethke (1959b), Halmann (1966) and Farmer et al. (1968) show good agreement except that the values by Farmer et al. (1968) are higher than others between v'=4 and 12. The values of Ditchburn and Heddle (1954) show extraordinary higher values for the whole vibrational levels. Theoretical values by Jarmain (1963), Harris et al. (1969) and Allison et al. (1971) are in good agreement with the experimental values, while those by Ory and Gittleman (1964), Halmann and Laulicht (1966) and Murrell and Taylor (1969) scatter widely from the experimental values.

In the following calculations we discuss the dissociation rates of molecular oxygen by two cases, using the values of Bethke (1959b), and the values of Farmer et al. (1968), where the experimental conditions are very different.

Bethke (1959b) obtained $K(v',v'')$ by pressure broadening the rotational lines with argon to the point where rotational structure disappeared, while Farmer et al. (1968) made the measurements under the conditions of very small attenuation which resolve adequately the rotational structure so that the observed absorption was directly proportional to the absorption coefficient. Adopted values in the following calculations are listed in Table 3. Values of Case A for $v''=0,1,18$, 19 and 20 are taken from Harris et al. (1969), the others are taken from Bethke(1959b). Values of Case B for $v''=0$, 1 are taken from Harris et al. (1969), the others are taken from Farmer et al. (1968).

In $v''=1$ progressions, Hudson and Carter (1968) measured the total band absorption oscillator strength $f(v',v'')$ for the range of $v'=5$ to 13. Ory and Gittleman(1964), Halmann and Laulicht (1966), Harris et al.(1969) and Allison et al.(1971) calculated the Franck-Condon factors theoretically. Integrated band absorption coefficients deduced by Equations (10) and (11) for 250°K are shown in Figure 8. Theoretical values by Harris et al. (1969) and Allison et al. (1971) agree well with the experimental values by Hudson and Carter(1968), while those by Ory and Gittleman(1964) and Halmann and Laulicht(1966) are considerably hihger than the experimental values. In this study we adopted the values of Harris et al. (1969) for the whole vibrational levels, which are listed in Table 3.

Integrated band absorption cross sections for $v''\geq 2$ progressions can be neglected because the fraction of the molecules in the lower vibrational state is very low even if the Franck-Condon factors are higher than those of $v''=0$ and $v''=1$.

4.5 Distribution of line intensities in a band

We assume in the present calculations a single P and a single R branch, each including three components of about the same intensity, and neglecte the weak satellite branches. Then, the distribution of intensities among the rotational lines of a vibrational transition is given by

$$S(N'';v',v'') = C_{abs}K(v',v'')\, N'' \exp[\, -B_{v''}N''(N''+1)ch/kT\,] \quad ; \text{ P branch} \quad (12)$$

$$S(N'';v',v'') = C_{abs}K(v',v'')(N''+1)\exp[-B_{v''}N''(N''+1)ch/kT] \quad ; \text{ P branch} \quad (12')$$

Here $S(N'';v',v'')$ is the integrated absorption coefficient over a certain triplet, $K(v',v'')$ is the integrated band absorption coefficient which was defined in the previous section, h is Planck's constant, k is Boltzmann's constant and C_{abs} is a constant. An example of the rotational structure of the Schumann-Runge bands around the wave number of 55250 cm^{-1} (1810 Å) at 250°K is shown in Figure 5.

4.6 Deduction of parameters for the random model

For the calculations of the dissociation rate of the oxygen molecule, we have divided the Schumann-Runge bands into 15 wavelength intervals by the band heads of the v''=0 bands as shown in Table 4. In each wavelength interval we used constant solar radiation, mean absorption coefficient of ozone and mean transmission.

(a) Distribution of line intensities

The intensities of rotational lines in the wavelength interval were calculated for v''=0 and v''=1 progressions. In each wavelength interval, the lines whose intensities are stronger than 10^{-4} of the intensity of the strongest line in the interval were taken into account. In Figure 9 intensity distributions for 15 wavelength intervals are shown. In this Figure the number of lines with intensity lower than S for each wavelength interval is plotted as a function of log S. The cumulative probability of lines with intensity lower than S, S_{cum},

is given by

$$S_{cum} = \int_{S_1}^{S} p(S)dS$$

where S_1 is the lowest value of S considered. For the probability function p(S) given by Equations (4),(6), (8) and (9), S_{cum} is shown schematically as a function of logS in Figure 10. Comparing Figure 9 with Figure 10, it is seen that the inverse first power distribution is most appropriate for the wavelength intervals 1 to 8. For the wavelength intervals 9 to 12 , the exponential distribution is more appropriate than the inverse first power distribution, while for the intervals 13 and 14 the inverse first power law is obeyed. For the interval 15 the constant probability distribution is more appropriate than other distributions. It is then concluded that the inverse first power law or exponential distribution can be used as the representative distribution of the line intensities in the Schumann-Runge bands.

(b) Mean line half-width

Line half-widths have been known only for v'-0 bands but have not been known for v'-1 bands, so we selected the following two cases of the line half-width for the band model.

Case A ; Mean line half-width for each wavelength interval was calculated only from the half-widths of the v'-0 bands.

Case B ; The line half-width of v'-1 band was assumed to be same as that of v'-0 band. Mean line half-width was calculated by taking both bands into account.

All the lines in a band were assumed to have the same half-width for both cases. Source data were taken from Hudson and Mahle (1972). Mean line half-widths, $\bar{\alpha}$'s, for two cases are shown in the 4th and 5th columns of Table 4.

(c) Mean line intensity (Mean absorption coefficient)

Mean line intensity in each wavelength interval was calculated using Equations (12) and (12'). For the calculations of the transmission, the mean absorption coefficient $\bar{k}$, defined by

$$\bar{k} = \bar{S} / \bar{d} \qquad (13)$$

is the more convenient parameter. $\bar{k}$ was calculated from

$$\bar{k} = \sum_{N''v'v''} S(N'';v',v'') / \Delta\nu \qquad (14)$$

where $\Delta\nu$ (cm^{-1}) is the wavenumber interval and $\sum_{N''v'v''} S(N'';v',v'')$ is the summation of the contributions of the rotational lines from all the bands within the wavenumber interval $\Delta\nu$. We considered the following two cases for the mean absorption coefficient corresponding to the two cases of the integrated absorption coefficients from the discussion in section 4.4.

Case A : Integrated absorption coefficients were taken from

K(v',0) : v'=2~17 ; Bethke (1959b)

v'=0,1,18~20 ; Calculated from q(v',0) by Harris et al.(1969)

K(v',1) : v'=0~20 ; Calculated from q(v',1) by Harris et al.(1969)

Case B : Integrated absorption coefficients were taken from

K(v',0) : v'=2~20 ; Farmer et al. (1968)

v'=0,1 ; Calculated from q(v',0) by Harris et al.(1969)

K(v',1) : v'=0~20 ; Calculated from q(v',1) by Harris et al.(1969)

The mean absorption coefficient, $\bar{k}$, calculated for the above two cases is shown in Table 4.

(d) Mean line spacing

The mean line spacing was calculated by counting all the spectral lines in each wavelength interval using Equation (1). In the present paper the

spectral lines whose intensity ratios to the strongest line in each wavelength interval are lower than 10^{-4} were neglected. The mean line spacing can have the different value if we take the spin splitting into cosideration. The triplet splittings for the lines of $v' \leq 11$ are very small and have not been completely resolved, while for $v' \geq 12$ the triplet splittings have been resolved and they increase with v' (Brix and Herzberg,1954 ; Ackerman and Biaumé,1970). In this report we considered following three cases for the line splittins.

Case A : All the lines are singlet.

Case B : Lines for $v' \leq 11$ are singlet, while
Lines for $v' \geq 12$ are triplet.

Case C : All the lines are triplet.

The mean line spacing , $\bar{d}$, of each wavelength interval is given in Table 4.

4.7 Photodissociation rate

4.7.1 Wavelength region out of the Schumann-Runge bands

The photodissociation rate of the light-absorbing species s in the wavenumber interval $(\nu, \nu + d\nu)$ is given by

$$J(s,\nu)d\nu = \varepsilon(s,\nu)\, F_\nu(\infty)\, T_\nu \sigma(s,\nu)d\nu$$

where $\varepsilon(s,\nu)$ is the quantum yield of primary photodissociation for the species s, $F_\nu(\infty)$ is the photon flux outside the atmosphere per cm^2 per second per wavenumber, T_ν is the transmission between the point in question and the sun, $\sigma(s,\nu)$ is the absorption cross section of the species s in cm^2/molecule. Transmission T_ν is given by

$$T_\nu = \exp\left[- \sum_s \sigma(s,\nu)\, N(s)\right]$$

where N(s) is the column density of the species s between the point in question and the sun. The dissociation rate of the species s for the whole wavenumber region out of the Schumann-Runge bands is given by

$$J(S) = \int J(s,\nu)d\nu\,, \qquad (15)$$

In this report we considered the oxygen and ozone molecules as the light absorbing species.

4.7.2 The Schumann-Runge bands

The dissociation rate of the species s in the i-th wavelength interval, $J_i(s)$, is calculated from

$$J_i(s) = - \varepsilon_i(s)\, F_i(\infty)\, \frac{\partial \bar{T}_i}{\partial N(s)} \qquad (16)$$

where $\varepsilon_i(s)$ is the quantum yield of the primary photodissociation for the species s in the i-th wavelength interval, $F_i(\infty)$ is the mean photon flux outside

the atmosphere per cm^2, per second in the i-th wavelength interval, and $\bar{T}_i$ the mean transmission in the i-th wavelength interval.

Dissociation rates for the exponential and inverse first power distribution of line intensities are deduced from the transmission function given in section 4.3. In this section the allowance was made for the transmissions of ozone and the underlying continuum of oxygen molecule.

(a) Exponential distribution of line intensitis

From the Equation (5) ,the mean transmission in the i-th wavelength interval is given by

$$\bar{T}_i = \exp\left\{-\frac{\bar{\sigma}(O_2)N(O_2)}{\sqrt{1+CN(O_2)}}\right\}\cdot\exp\left\{-\sigma_c(O_2)N(O_2)\right\}\cdot\exp\left\{-\sigma(O_3)N(O_3)\right\} \qquad (17)$$

where $\bar{\sigma}(O_2)$ is the mean absorption cross section of the oxygen molecule, $\sigma_c(O_2)$ is the underlying continuum absorption cross section of oxygen molecule, $\sigma(O_3)$ is the mean absorption cross section of the ozone, and $N(O_2)$ and $N(O_3)$ are the total numbers of oxygen and ozone per cm^2 in the light path, respectively. $\bar{\sigma}(O_2)$ is related to the mean absorption coefficient of oxygen molecules $\bar{k}$ as

$$\bar{\sigma}(O_2) = \bar{k} / n_o$$

where n_o is the Loschmidt's number. ($n_o = 2.6874\times10^{19}$ particles cm^{-3}).
Here C stands for

$$C = \bar{\sigma}(O_2)\,\bar{d} / \Pi\bar{\alpha}.$$

From Equations (16) and (17), the dissociation rate of the oxygen molecule is given by

$$J_i(O_2) = \varepsilon_i(O_2)\cdot F_i(\infty)\cdot\bar{T}_i\cdot\left[\frac{\bar{\sigma}(O_2)\left\{1+\frac{1}{2}CN(O_2)\right\}}{\left\{1+CN(O_2)\right\}\sqrt{1+CN(O_2)}} + \sigma_c(O_2)\right] \qquad (18)$$

and the dissociation rate of the ozone molecule is given by

$$J_i(O_3) = \varepsilon_i(O_3)\, F_i(\infty)\, \bar{T}_i\, \sigma(O_3) \qquad (19)$$

where $\bar{T}_i$ is given by Equation (17).

(b) Inverse first power distribution

From Equations (2) and (7) the mean transmission is given by

$$\bar{T}_i = \exp\left[-\frac{\bar{\sigma}(O_2)}{u_o}\left\{I_0(u)\exp(-u) + 2u\left(I_0(u) + I_1(u)\right)\exp(-u) - 1\right\}\right]\cdot$$

$$\exp\left\{-\sigma_c(O_2)N(O_2)\right\}\exp\left\{-\sigma(O_3)N(O_3)\right\} \qquad (20)$$

where $u_o = \bar{d}\,\bar{\sigma}(O_2)/2\Pi\bar{\alpha}\,K$. K is a constant introduced in Equation (6) and is determined as follows. Integration of the probability function gives

$$\int_{S_1}^{S_2} p(S)dS = \int_{S_1}^{S_2}\frac{k}{S}dS = K\ln\left(\frac{S_2}{S_1}\right) = 1 .$$

As was stated in section 4.5(d), the ratio of S_2 to S_1 was chosen as $S_2/S_1 = 10^4$. Then K becomes

$$K = 0.10857.$$

From Equations (16) and (20), the dissociation rates of oxygen molecule $J_i(O_2)$ and ozone molecule $J_i(O_3)$ are given by

$$J_i(O_2) = \varepsilon_i(O_2)\cdot F_i(\infty)\cdot\bar{T}_i\cdot\left[\bar{\sigma}(O_2)\left\{I_0\left(u_oN(O_2)\right) + I_1\left(u_oN(O_2)\right)\right\}\exp\left(-u_oN(O_2)\right) + \sigma_c(O_2)\right] \qquad (21)$$

$$J_i(O_3) = \varepsilon_i(O_3)\,F_i(\infty)\,\bar{T}_i\,\sigma(O_3) \qquad (22)$$

where $\bar{T}_i$ is given by Equation (20).

5. Results

For the calculation of the dissociation rates of the oxygen molecule, continuum absorption coefficients of oxygen molecules were taken from Hudson and Mahle (1972) in the wavelength region 1750 - 1950 Å, and from Ditchburn and Young (1962) above 1950 Å. Absorption coefficients of ozone was taken from Inn and Tanaka (1959) above 2000 Å and from Watanabe (1958) below 2000 Å. The total number of the oxygen molecules above a given height was calculated from the data of U.S. Standard Atmosphere Supplements (1966) for 30°N lat January, supposing the proportion of the oxygen molecules to be 20.95 % by volume and is shown in Table 5. Mean vertical ozone distribution for 30° N lat, winter was assumed as shown in Table 5 with reference to the rocket and the satellite observations (WU,1973).

5.1. Effect of the predissociation

The effect of the predissociation on the photodissociation rate of the oxygen molecule was estimated under the condition that the oxygen molecule that is excited into the $B^3\Sigma_u^-$ state for $v' > 2$ is completely predissociated. This is equivalent to giving $\varepsilon_i(O_2)$ in Equation (16) the value of unity for i-th wavelength interval corresponding to $v' > 2$. The solid curves in Figure 11 show the vertical distribution of the dissociation rate of oxygen molecule when the predissociation was taken into account at secz=1,3, 6,where z is the solar zenith angle. The broken curves show the corresponding values when the predissociation was neglected while the dissociation by underlying continuum was taken into account. Figure 11 shows the result under the condition that solar radiation is Case B, the distribution of line intensities is inverse first power i.e. $p(S) = K/S$, line parameters $\bar{k}$, $\bar{d}$, $\bar{\alpha}$ are Case A, Case B, Case B of which values are shown in Table 4, respectively.

The appreciable contributions of the predissociation appear above 45 km. The maximum contribution appears at 75 km for secz = 1.0, at 80 km for secz=3.0 and at 85 km for secz=6.0. The ratio of the dissociation rate including predissociation to that neglecting predissociation has the maximum value of 3.4 for each case shown in Figure 11. The vertical distributions of this ratio of the dissociation rate for various cases of the solar radiation, the distribution of line intensities and band model parameters at secz =3.0 are shown in Figure 12. The solid curves (1), (2), (3) and (4) show the ratios for the solar radiation of Case B. The dashed curves (1'), (2'), (3') and (4') show the ratios for the solar radiation of Case C whose data have been obtained by the photoelectric technique and show the lower intensities than Case B.

It is seen from the curves in Figure 12 :

(a) The effect of the predissociation is larger for the higher intensities of the solar radiation. (Compare the curves (1) with (1'), and (2) with (2') and so on.)

(b) For the distribution of line intensities the effect of the predissociation is larger for the inverse first power distribution than the exponential distribution. (Compare the curves (1) with (2) , (3) with (4), (1') with (2') and (3') with (4').)

(c) The effect of the predissociation is larger for the higher mean absorption coefficient $\bar{k}$. (Compare the curves (1) with (3), (2) with (4), (1') with (3') and (2') with (4').)

(d) The maximum effect of the predissociation appears at 80 km for all cases when secz = 3.0.

(e) The maximum value of the ratio of the dissociation rate including predissociation to that neglecting predissociation amounts to 7.82 at 80 km for secz = 3.0 under the conditions; solar radiation =Case A, p(S)= inverse first power distribution, $\bar{k}$=Case B, $\bar{d}$= Case C, $\bar{\alpha}$ =Case B.

5.2 Effect of the solar radiation

The large differences are recognized among the repoted solar radiations below 2500 Å, so we selected three cases of the solar radiation from the discussions in section 3 to see the influences on the dissociation rate of oxygen molecule.

Case A : Data from the old measurements by NRL group (photographic technique).

Case B : Data depending on the new measurements by NRL group(Widing et al.1970) which show a lower intensity than the old data in the Schumann-Runge region ,(photographic technique).

Case C : Data depending on the measurements by the photoelectric technique whose intensity is lower by a factor of 3 to 2 than that of Case A in the Schumann-Runge region.

Vertical distributions of the dissociation rate of the molecular oxygen were calculated for the solar radiation of Case A, Case B and Case C under the condition that the distribution of line intensities is the inverse first power law, $\bar{k}$ is Case A, $\bar{d}$ is Case C and $\bar{\alpha}$ is Case B. Calculated results are shown in Figure 13. The ratio of the dissociation rate for Case A of the solar radiation to that for the Case C shows the maximum value of 4.10 at 100 km and reaches the minimum value of 2.35 at 45 km. The ratio of this for Case B to Case C is 2.57 at 100 km and 2.06 at 50 km. Above ratio for the exponential distribution of line intensities show almost the same values as those for the inverse first power distribution.

We can conclude from the above discussions that the ambiguity of the photodissociation rate of the oxygen molecule caused by the uncertainty of the solar radiation intensity is a factor of 2 to 4 between 40 and 100 km.

5.3 Effect of the distribution function of line intensities

From the discussions of the section 4.6, we came to the conclusion that in the Schumann-Runge region the distribution of the line intensities can be represented by the inverse first power or the exponential distribution. Vertical distributions of the calculated dissociation rate of the oxygen molecule for

the two types of the distribution , assuming the other line parameters to be same, are shown in Figure 14. The solid curves (a), (b), and (c) show the dissociation rates for the inverse first power distribution and the dashed curves (a'),(b') and (c') show those for the exponential distribution. The difference of dissociation rates for the two distributions increases with the altitude. The dissociation rate for the exponential distribution is higher by 10 to 11 % at 100 km while it is lower by 2 to 4 % at 40 km for the solar radiation of Cases A,B,C and secz=1 $\sim$ 3. If the predissociation is neglected the dissociation rate of the molecular oxygen for the exponential distribution is higher by 1$\sim$4 % than for the inverse first power distribution betweem 40 and 100 km.

It is then concluded that the deviation due to the distribution function is at most about 11 % between 40 and 100 km.

5.4 Effect of the band model parameters

The mean transmission by the band model is determined by the mean absorption coefficient $\bar{k}$, mean line spacing $\bar{d}$ and mean line half-width $\bar{\alpha}$. The values of these parameters were discussed in section 4.6 and the representative cases were selected for the each parameter. The deviations of the dissociation rate of the molecular oxygen due to the variations of the line parameters were estimated for the two distribution functions of line intensities i.e. exponential and inverse first power distribution.

(a) Mean absorption coefficient

In section 5.6 two cases were assumed for the mean absorption coefficient of the Schumann-Runge bands. In Case A integrated absorption coefficients for v'' = 0 were taken from Bethke (1959b). while in Case B the values by Farmer et al. (1968) were adopted. Small contributions from v'' = 1 progression were calculated from the Franck-Condon factors given by Harris et al. (1969) for both Cases. Figure 15 shows the variation of the dissociation rate of the molecular oxygen due to the variation of the mean absorption coefficient. Curve (a) and

(b) show the dissociation rate for Case A and Case B of the mean absorption coefficient $\bar{k}$, assuming other parameters to be same i.e. Csae B for the solar radiation, inverse first power distribution for line intensities, Case B for the mean line spacing $\bar{d}$, Case B for the mean line half-width and secz=1.0. Curves (c) and (d) show the corresponding values for the Case C of the solar radiation. Above 60 km dissociation rates of the Case B of the mean absorption coefficients show the higher values than for the Case A and the maximum difference is about 20 % at 75 km. This tendency can be expected from the higher mean absorption coefficients of Case B compared with Case A. Below 55 km, on the other hand, the dissociation rates for the Case B are lower than for the Case A, and the maximum difference is about 3 %. These tendency and the magnitude of the deviations of the dissociation rates are almost same for the exponential distribution of line intensities and for secz=1 ∿ 3.

Integrated absorption coefficients adopted for the Case B of the mean absorption coefficients are higher than those for the Case A by a factor of 4 at $v' = 5$ as shown in Table 3. It is seen that the deviation of the dissociation rate owing to the deviation of the mean absorption coefficient is rather small compared with the deviation of the latter. It is also seen that the deviation owing to the uncertainty of the solar radiation is considerably larger (amounting to a factor of 4) than the deviation owing to the mean absorption coefficients.

(b) Mean line spacing

We assumed three cases for the mean line spacing considering the spin splitting of the spectral line as discussed in section 4.6 and shown in Table 4. The vertical distributions of the dissociation rate of the molecular oxygen for the three cases of the mean line spacing $\bar{d}$ are shown in Figure 16. Two groups of the curves are drawn for the different solar radiation, Case B (curves (a), (b), (c)) and Case C (curves (d),(e),(f)). The triplet splittings of lines

for $v'' \leq 11$ are very small and have not been completely resolved while they have been resolved for $v'' \geq 12$, so Case B of the mean line spacing $\bar{d}$ is more appropriate than Case A or Case C. In Case A the triplet splittings are completely neglected, while in Case C all the lines are assumed to be triplets, so Case A and Case C the extreme cases.

It is seen from the Figure 16 that the dissociation rates of the molecular oxygen for Case C of $\bar{d}$ are higher than for Case B of $\bar{d}$ above 60 km but lower below 60 km.(Compare curve (c) with (b) or curve (f) with (e),). The deviation of the dissociation rate of oxygen molecule for these two cases shows the maximum value of 17 % at 75 km for secz=1.0. The height of the maximum deviation increases with secz and reaches 85 km for secz = 3.0. The dissociation rates for Case A of $\bar{d}$ is lower than for Case B of $\bar{d}$ above 75 km and higher below 75 km. (Compare curve (a) with (b) and curve (d) with (e).) The maximum deviation is about 13 % at 100 km. The magnitude and the tendency of the above-mentioned deviation due to the mean line spacing are almost constant for any cases of the solar radiation and the distribution function of line intensities. It is also seen that the uncertainty of the dissociation rate due to the mean line spacing is considerably lower than the uncertainty due to the solar radiation.

It is concluded that the deviation of the dissociation rate of the oxygen molecule due to the mean line spacing is lower than 20 % below 100 km.

(c) Mean line half-width

As the line-widths of v'-1 bands have not been known, the mean line half-widths of Case A were deduced from solely the half-widths of v'-0 bands. In Case B, line half-widths of v''=1 progression were assumed to be same as those of v''=0 progression, and the mean line half-widths were deduced from both progressions. Figure 17 shows the example of the dissociation rates of oxygen molecule for Case A and Case B of the mean line half-width $\bar{\alpha}$ under the conditions ; $F_\nu(\infty)$=Case C and Case B, p(S)=K/S, $\bar{k}$=Case B, $\bar{d}$=Case B and secz = 1.0. The dissociation

rate for Case A of the line half-width is higher than for Case B above 65 km, but lower below that height. (Compare curve (a) with (b) or curve (c) with (d)). The maximum deviation is about 5 % at 85 km. Below 65 km the deviation is lower than 3 %. The height of the maximum deviation increases with the solar zenith angle, but the magnitude of the deviation remains almost unchanged. These results remain unaltered if the distribution function is changed to the exponential distribution.

It is then concluded that the deviation of the dissociation rate of the oxygen molecule due to the mean line half-width is about 5 % at most.

5.5 Comparison with other calculations

Hudson et al. (1969) made the laboratory determination of the dissociation rate of the molecular oxygen and applied the results to the atmosphere. Hudson and Mahle (1972) performed the line-by-line calculation of the band-absorption cross sections as a function of the column density of oxygen molecules and compared their results with those obtained from the measurements by Hudson et al. (1969).They state that for all wavelength intervals the agreement is well within the experimental error. The photodissociation rate of the molecular oxygen with inclusion of the effect of the predissociation in the Schumann-Runge bands obtained by Hudson et al. (1969) is shown by the dashed curve in Figure 18. The original data are shown as a function of the column density of the oxygen molecules but in this Figure the data are shown as a function of the height using the height-column density relation corresponding to 30°N January of U.S. Standard Atmosphere Supplements (1966). The dashed-dotted curve in Figure 18 is the results of Fang et al. (1974) calculated using the opacity distribution functions in the Schumann-Runge bands. They used the oscillator strength which is nearly the same as that of Hudson and Mahle (1972). Furthermore, Fang et al. (1974) used the data of the line half-width given by Hudson and Mahle (1972). Two curves obtained by Hudson et al. (1972) and Fang et al.(1974) are in good agreement. The solid

curves (a), (b), (c) and dotted curves (a'), (b'), (c') in Figure 18 show the values obtained by the random model approximation for Cases A, B, C of the solar radiation $F_\nu(\infty)$, and for Cases A and B of the mean absorption coefficient $\bar{k}$. Curve (b) shows the smallest deviation from the curve of Fang et al. (1974). This is expected from the fact that the data of the oscillator strength and of the line half-width used in both calculations are very similar. Curve (b) shows the higher photodissociation rate than that of Fang et al. (1974) below 95 km, while it shows the lower values above 95 km. The maximum deviation is about 70 % around 85 km. Fang et al. (1974) used the solar radiation slightly lower than ours used in Case B of the solar radiation. Another difference between our data and those of Fang et al. (1974) is the atmosphere model. Fang et al. (1974) used the data of the atmosphere from U.S. Standard Atmosphere Supplements (1966) for 30°N lat, July, while we used those for 30°N lat, January. The column density of the oxygen molecules is large in July than in January between the altitude of 10 and 90 km. The maximum difference is about 15 % around 70 km. So if we use the atmosphere for July the dissociation rates are lowered in proportion to the deviation of the column density of the oxygen molecules below the altitude of 90 km, and the difference between curve (b) and the curve of Fang et al. (1974) would be reduced. The curves (c) and (c') show the values for the same solar radiation $F_\nu(\infty)$ of Case C and for different value of the mean absorption coefficient $\bar{k}$, i.e. for the $\bar{k}$ of Case A (curve (c)) and Case B (curve (c')). It is seen that the difference between the curve (b) and the curve of Fang et al. (1974) is smaller than that between the curve (b) and curve (c). The former difference is due to the difference in the method of the calculations of the transmission of the solar radiation in the Schumann-Runge bands, while the latter difference is due to the uncertainty of the solar radiation.

It is said that the ambiguity of the dissociation rate due to the uncertainty of the solar radiation is significantly larger than that due to the calculation method of the transmission.

5.6 Dissociation rate by the average band-absorption coefficient

The calculation of the photodissociation rate of the oxygen molecule in the Schumann-Runge bands can be considerably simplified if we can use the average band-absorption coefficient neglecting the rotational structure of the bands. In this section we calculated the vertical distribution of the photodissociation rate of the oxygen molecule for the average band-absorption coefficients assuming Lambert-Beer's law and compared the results with that deduced from the band model. In Figure 19 three stepwise curves (1), (2) and (3) are shown. Curve (1) is drawn so as to connect the bottoms of the absorption coefficient of the band shown in Figure 4, or it may be regarded as the apparent underlying continuum. Curve (3) shows the mean absorption coefficient $\bar{k}$ of Case A adopted in the band model. Curve (2) was chosen so that the photodissociation rate of the oxygen molecule from curve (2) nearly coincides with the rate deduced from the band model. (See Figure 20). Figure 20 shows the dissociation rates of the oxygen molecule calculated by the average band-absorption coefficient shown in Figure 19. Solid curves (b) and (c) show the values deduced from the random model for Cases B and C of the solar radiation $F_\nu(\infty)$ respectively, under the conditions; the exponential distribution of the line intensities, Case A for $\bar{k}$, Case B for $\bar{d}$ and Case B for $\bar{\alpha}$. Curves (b_1), (b_2) and (b_3) show the values corresponding to the average band-absorption coefficients of (1). (2) and (3) in Figure 19 for the solar radiation of Case B at secz = 3. Curves (c_1), (c_2) and (c_3) show the corresponding values for the solar radiation of Case C. The deviation of (c_1) and (c_3) from (c) increases with height and reaches $\pm$ 25 % at 100 km. This deviation is maximum when secz = 1 and decreases with increasing secz. When the average band-absorption coefficient of curve (2) in Figure 19 is used, the vertical distribution of the dissociation rate of the oxygen molecule nearly coincides with the value deduced from the random model approximation using the curve (3) in Figure 19 for $\bar{k}$.

It is said that the dissociation rate of the oxygen molecule between 40 and 100 km can be calculated by the appropriate average band-absorption coefficient (for example, curve (2) in Figure 19) in the Schumann-Runge bands.

5.7 Dissociation rate of the ozone molecule

Photodissociation of the ozone molecule occurs by the light absorption mainly in the Hartley band from 2000 to 3000 Å in the stratosphere and mesosphere. As the Hartley band and the Schumann-Runge bands do not overlap, the calculated dissociation rate of the ozone is almost independent of the predissociation and the band model approximation in the Schumann-Runge bands for the oxygen molecule discussed above, but is somewhat influenced by the uncertainty of the solar radiation.

The vertical distribution of the dissociation rate of the ozone calculated by Equations (15) and (22) is shown in Table 6 for the solar radiation of Cases A, B, and C at secz = 1, 3 and 6. As the intensities of the solar radiation $F_\lambda(\infty)$ of Cases A and B are taken to be equivalent between 2000 and 2500 Å, the dissociation rates of the ozone molecule for these cases nearly coincide. Furthermore, it is seen from Table 6 that the dissociation rate of the ozone for Case C of the solar radiation is lower than that for Case A or Case B and the deviation increases with height below 60 km, but remains at 6 % for secz = 1, 3 and 6 above 60 km.

It is then concluded that ambiguity in the photodissociation rate of atmospheric ozone due to the uncertainty of the solar radiation is less than 6 % between altitudes of 40 and 100 km.

5.8 Vertical distribution of ozone

Vertical distributions of ozones were calculated in a pure oxygen atmosphere to see the effect of the predissociation of the oxygen molecule and the deviation of the solar radiation. In the pure oxygen atmosphere photochemical ozone is formed and reduced by the following reactions :

$$O_2 + h\nu \longrightarrow 2O \qquad J(O_2)$$

$$O_3 + h\nu \longrightarrow O_2 + O \qquad J(O_3)$$

$$O + O + M \longrightarrow O_2 + M \qquad k_1$$

$$O + O_2 + M \longrightarrow O_3 + M \qquad k_2$$

$$O + O_3 \longrightarrow 2O_2 \qquad k_3$$

where $J(O_2)$, $J(O_3)$ are the dissociation rates of oxygen and ozone molecules respectively, and k_1, k_2 and k_3 are the rate constants for the reactions. Adopted values of the rate constants are

$k_1 = 3.80\times10^{-30}T^{-1}\exp(-170/T)$ $cm^6 molec^{-2} sec^{-1}$ Garvin and Hampson (1974) review

$k_2 = 1.06\times10^{-34}\exp(+510/T)$ $cm^6 molec^{-2} sec^{-1}$ Garvin and Hampson (1974) review

$k_3 = 1.9\times10^{-11}\exp(-2300/T)$ $cm^3 molec^{-1} sec^{-1}$ Garvin and Hampson (1974) review

The effect of the excited state of the oxygen atom $O(^1D)$, which was considered in the previous calculation (Muramatsu et al. 1971), is very small. In this calculation $O(^1D)$ was assumed to be quenched to $O(^3P)$ immediately.

Figure 21 shows the ozone profiles for the atmosphere of 30°N winter (mean solar zenith angle of 60°). Solid curves (a) and (a') are the ozone profiles for the solar radiation of Case B, and the dashed curves (b) and (b') are for the solar radiation of Case C. Curves (a) and (b) show the ozone profiles obtained when the predissociation of oxygen molecule was taken into account and curves (a') and (b') show the profiles obtained by neglecting the predissociation. Parameters for the random model are p(S)=inverse first power, $\bar{k}$ = Case A, $\bar{d}$ = Case B, and $\bar{\alpha}$ = Case B.

Two dotted curves show the range of observations of the ozone which contains practically all profiles compiled by Wu (1973). The ozone concentration with predissociation of the oxygen molecule is higher than that without predissociation above 55 km and the deviation is maximum between 75 and 80 km by a factor of 2 for Case B of the solar radiation (compare curve (a) with (a')), and a factor of 1.6 for Case C (compare curve (b) with (b')). On the other hand , the ozone concentration for Case B of the solar radiation is higher than that for Case C by a factor of 1.5 above 30 km (compare curve (a) with (b)).

Comparing with the range of the observations of the ozone, the calculated ozone profile for Case B of the solar radiation, curve (a), comes out of the range between 25 and 40 km and above 65 km, while the ozone profile for Case C, curve (b), comes out of the range only above 70 km. So it is said that the solar radiation of Case C gives better fit with observations than that of Case B, but the great discrepancy appears above 65 km. This discrepancy cannot be explained by the uncertainties of the solar radiation or the predissociation of the Schumann-Runge bands of the oxygen molecule. It may be explained by other effects, i.e. transports (eddy diffusion, advection),minor constituents (hydrogen compounds and nitrogen compounds) or by the uncertainty of the rate constants. Discrepancy between 30 and 40 km may be caused mainly by the minor constituents.

6. Summary and concluding remarks

Photodissociation rates of the oxygen and ozone molecules in the stratosphere, mesosphere and lower thermosphere were examined to see ambiguities in computed rate due to the uncertainties in the predissociation in the Schumann-Runge bands, the solar radiation intensity and the transmission in the Schumann-Runge bands. The estimation of these influence on the calculated distribution of the ozone molecule was made to examine if these uncertainties may be the cause of the discrepancy between the observed and theoretical profiles of the atmospheric ozone.

The vibrational levels of the $B^3\Sigma_u^-$ state are predissociated to some extent between v'=3 and v'=17. This has been confirmed by the spectroscopic and photochemical evidences but various questions remain to be solved ; the crossing point of the potential curve of the $^3\Pi_u$ state with that of the $B^3\Sigma_u^-$ state, contributions of the other repulsive states $^5\Pi_u$, $^5\Sigma_u^-$ and $^1\Pi_u$, the contribution of the underlying continuum to the decomposition of the oxygen molecule, the quantum yield of the ozone formation from the decomposition of the excited oxygen molecule in the Schumann-Runge bands and so on. More detailed experimental information, especially of the line half-width is necessary to solve these questions.

Large variations are recognized among the reported solar ultraviolet radiations below 2500 Å. These variations may be caused by the absolute intensity calibration, the difference of the detectors and the variability of the solar radiation i.e. time variation and spatial variation. The solar spectral intensities measured by the photoelectric technique are in general lower by a factor of 3 than those by the photographic technique in the wavelength region below 2000 Å. The cause of the difference has not been known.

To extent of the ambiguity caused by inevitable uncertainties in solar radiation intensity and so on, the random model gives a reasonable result in accuracy as same as the exact calculation.

The appreciable effect of the predissociation to the dissociation rate of the oxygen molecule appears above 45 km. The altitude of the maximum effect is

found at 75 km for secz=1 and it increases with secz. The ratio of the dissociation rate including the predissociation to that neglecting the predissociation falls in the range from 8 to 3.

The uncertainty of the solar intensity gives ambiguity of a factor 2 to 4 to the dissociation rate of the oxygen molecule between 40 and 100 km.

The dissociation rate of the oxygen molecule computed with band model for the Schumann-Runge bands is influenced somewhat by the selection of the model parameters. Their influences are about 11 % from the selection of the distribution function, 20 % from the mean line spacing, 20 % from the line intensity, and 5 % from the line half-width. Last two influences are caused mainly from the ambiguity of the experimental data adopted. Ambiguities in the band model are fairly small compared with those caused from the solar radiation intensity and the predissociation effect.

The photodissociation rate of the ozone molecule is little affected by the predissociation or by the selection of the band model for the Schumann-Runge bands but has the uncertainty of about 6 % due to the ambiguity of the solar radiation intensity.

Vertical distributions of the ozone molecule in a pure oxygen atmosphere were calculated for the various combinations of the parameters. The profile deduced from the solar radiation obtained by the photoelectric technique, neglecting the predissociation of the oxygen molecule in the Schumann-Runge bands gives rather better fit with the observed profiles. Some difference is recognized between the observed and calculated profile above 65 km, and this difference cannot be explained by the uncertainties discussed in the present paper only. The photochemical theory of the atmospheric ozone should be refined by the improvement of the knowledge of the parameters with allowance of the effect of minor constituents and the eddy diffusion. Observations and monitoring of the solar radiation in the Schumann-Runge region are important from the above mentioned reasons.

Acknowledgement The author would like to acknowledge the helpful suggestions and encouragement of Professor R. Yamamoto of Kyoto University and Dr. K. Sekihara, Chief of the Upper Atmospheric Physics Laboratory of the Meteorological Research Institute.

References

Ackerman,M. and F. Biaumé, 1970: Structure of the Schumann-Runge bands from 0-0 to the 13-0 band. J.Molecular Spectroscopy, 35, 73-82.

Ackerman,M.,F.Biaumé and G Kockarts, 1970: Absorption cross sections of the Schumann-Runge bands of molecular oxygen. Planet. Space Sci., 18, 1639-1651.

Allison, A.C., A. Dalgarno and N.W.Pasachoff, 1971: Absorption by vibrationally excited molecular oxygen in the Schumann-Runge continuum. Planet. Space Sci., 19, 1463-1473

Bethke,G.W., 1959a: Oscillator strengths in the far ultraviolet.I. Nitric oxide. J.Chem.Phys.,31,662-668.

Bethke,G.W., 1959b: Oscillator strengths in the far ultraviolet.II. Oxygen Schumann-Runge bands. J.Chem.Phys.,31,669-673.

Bonnet,R., 1968: Recherches sur l'émission continue du soleil entre 1950 et 3000Å. Ann. Astrophys., 31,597-644.

Brewer,A.W. and A.W.Wilson, 1965: Measurements of solar ultraviolet radiation in the stratosphere. Quart.J.R.Met.Soc.,91,452-461.

Brix,P. and G.Herzberg, 1954: Fine structure of the Schumann-Runge bands near the convergence limit and the dissociation energy of the oxygen molecule. Can. J. Phys.,32,110-135.

Brueckner,G.E. and O.K.Moe, 1972: High angular resolution absolute intensity of the solar continuum from 1400A to 1790A. Space Res.,12,1595-1602.

Carroll,P.K., 1959: Predissociation in the Schumann-Runge bands of oxygen. Astrophys. J.,129,794-800.

Crutzen,P.J., 1970: The influence of nitrogen oxides on the atmospheric ozone. Quart.J.R.Met.Soc.,96,320-325.

Detwiler,C.R.,D.L.Garrett,J.D.Purcell and R.Tousey, 1961: The intensity distribution in the ultraviolet solar spectrum. Ann. Géophys., 17, 263-272.

Ditchburn,P.W. and D.W.O.Heddle, 1954: Absorption cross-section in the vacuum ultra-violet.II. The Schumann-Runge bands of oxygen.(2000 to 1750Å) Proc. Roy. Soc. A.,226,509-521.

Ditchburn, R.W. and P.A.Young, 1962: The absorption of molecular oxygen between 1850 and 2500 Å, J.Atmos. Terr.Phys., 24, 127-139.

Dupree, A.K., M.C.E.Huber, R.W.Noyes, W.H.Parkinson, E.M.Reeves and G.L.Withbroe, 1973: The extreme-ultrviolet spectrum of a solar active region, Astrophys. J., 182, 321-333.

Fang,T.M.,S.C.Wofsy and A.Dalgarno, 1974: Opacity distribution functions and absorption in Schumann-Runge bands of molecular oxygen. Planet. Space Sci., 22, 413-425.

Farmer,A.J.D.,W.Fabian, B.R.Lewis, K.H.Lokan and G.N.Haddad, 1968: Experimental oscillator strengths for the Schumann-Runge band system in oxygen, J.Quant. Spectrosc. Radiat. Transfer, 8, 1739-1746.

Flory, P.J.,1936: Predissociation of the oxygen molecule. J.Chem. Phys., 4, 23-27.

Garvin,D.,and R.F.Hampson, 1974: Chemical kinetics data survey VII. Tables of rate and photochemical data for modelling of the stratosphere. (revised), NBSIR-74-430,Washington, D.C. 20234. 101p.

Goody, R.M.,1964: Atmospheric Radiation I. Oxford University Press. London, pp. 67-170.

Hall,L.A.,J.E.Higgins,C.W.Chagnon, and H.E.Hinteregger, 1969: Solar-cycle variation of extreme ultraviolet radiation. J.Geophys. Res.,74, 4181-4183.

Halmann,M., 1966: Isotope effects on Frank-Condon factors. VI.Pressure-broadened absorption intensities of the Schumann-Runge bands of $^{16}O_2$ and $^{18}O_2$. J.Chem. Phys., 44, 2406-2408.

Halmann,M. and I.Laulicht, 1966: Isotope effects on Franck-Condon factors. V. Electronic transitions of isotopic O_2,N_2,C_2, and H_2 molecules. J.Chem. Phys., 44, 2398-2405.

Harris,R.,M.Blackledge, and J.Generosa, 1969: Rydberg-Klein-Rees(RKR) Frank-Condon factors for the O_2 Schumann-Runge system including high vibrational quantum numbers. J.Molec. Spectros.,30, 506-512.

Heath,D.F.,1973: Space observations of the variability of solar irradiance in the near and far ultraviolet. J. Geophys. Res., 78, 2779-2792.

Herzberg,G., 1950: Spectra of Diatomic Molecules. D. van Nostrand Co., N.Y. 858p.

Hesstvedt,E., 1968a: On the effect of vertical eddy transport on atmospheric composition in the mesosphere and lower thermosphere. Geofys. Publ.,27, (4), 1-35.

Hesstvedt,E., 1968b: On the photochemistry of ozone in the ozone layer. Geofys. Publ., 27, (5), 1-16.

Hinteregger,H.E., 1970: The extreme ultraviolet solar spectrum and its variation during a solar cycle. Ann. Geophys., 26, 547-554.

Hudson,R.D.,1971: Critical review of ultraviolet photoabsorption cross sections for molecules of astrophysical and aeronomic interest. Rev. Geophys. and Space Phys.,9,305-406.

Hudson,R.D. and V.L. Carter, 1968: Absorption of oxygen at elevated temperatures (300 to 900 K) in the Schumann-Runge system. J. Opt. Soc. Am., 58, 1621-1629.

Hudson,R.D., V.L. Carter and E.L. Breig, 1969: Predissociation in the Schumann-Runge band system of O_2 : Laboratory measurements and atmospheric effects. J.Geophys. Res., 74, 4079-4086.

Hudson, R.D. and S.H. Mahle, 1972: Photodissociation rates of molecular oxygen in the mesosphere and lower thermosphere. J. Geophys. Res.,77,2902-2914.

Hunt,B.G., 1966a: The need for a modified photochemical theory of the ozonosphere. J. Atmos. Sci., 23, 88-95.

Hunt, B.G., 1966b: The photochemistry of ozone in a moist atmosphere. J. Geophys. Res., 71, 1385-1398.

Inn,E.C.Y. and Y.Tanaka, 1959: Ozone absorption coefficients in the visible and ultraviolet region. Advances in Chemistry, Ser. 21, 263-268.

Jarmain,W.R., 1963: Franck-Condon factors from Klein-Dunham potentials for the v" = 0 progressions of the Schumann-Runge system of O_2. Can. J. Phys.,41. 1926-1929.

Jarmain, W.R. and R.W. Nicholls, 1967: A theoretical stydy of the v'' = 0,1,2 progressions of bands and adjoining photodissociation continua of the O_2 Herzberg I system. Proc. Phys. Soc. 90, 545-553.

Johnson,F.S., 1954: The solar constant. J. Met., 11, 431-439.

Muramatsu,H., M.Kyozuka and M.Misaki, 1971: A rocket measurement of the vertical distribution of atmospheric ozone. Papers in Meteorology and Geophysics, 22, 209-227.

Murrell,J.N. and J.M. Taylor, 1969: Predissociation in diatomic spectra with special reference to the Schumann-Runge bands of O_2 Molec. Phys.,16, 609-621.

Nishi,N.,K.Higashi,A.Yamaguchi and Z.Suemoto, 1973: Observation of the absolute intensity and the centre-to-limb variations of the sun in the vacuum ultraviolet region.(in Japanese) Bulletin of the Institute of Space and Aeronautical Science, University of Tokyo, 9,359-376.

Ogawa,M., 1971: Absorption cross sections of O_2 and CO_2 continua in the Schumann and far-uv regions. J.Chem.Phys.,54,2550-2556.

Ory, H.A. and A.P. Gittleman, 1964: Unusual variation of Franck-Condon factors for the O_2 Schumann-Runge band system. Astrophys.J.,139,359-364.

Park,J.H., 1974: The equivalent mean absorption cross sections for the O_2 Schumann-Runge bands: Application to the H_2O and NO photodissociation rates. J. Atmos. Sci.,31, 1893-1897.

Parkinson,W.H. and E.M.Reeves, 1969: Measurements in the solar spectrum between 1400 and 1875 Å with a rocket-borne spectrometer. Solar Phys.,10,342-347.

Prag, A.B. and F.A.Morse, 1970: Variations in the solar ultraviolet flux from July 13 to August 9, 1968. J.Geophys. Res.,75, 4613-4621.

Rice, O.K., 1930: Perturbations im molecules and the theory of predissociation and diffuse spectra II. Phys. Rev., 35, 1551-1558.

Schaefer III,H.F.,and F.E. Harris, 1968: *Ab initio* calculations on 62 low-lying states of the O_2 molecule. J. Chem. Phys., 48, 4946-4955.

Schaefer III, H.F. and W.H. Miller, 1971: Curve crossing of the $B^3\Sigma_u^-$ and $^3\pi_u$ states of O_2 and its relation to predissociation in the Schumann-Runge bands. J.Chem. Phys.,55,4107-4115.

Thompson,B.A.,P. Harteck and R.R.Reeves,Jr., 1963: Ultraviolet absorption coefficients of CO_2, $CO,O_2,H_2O,N_2O,NH_3,NO,SO_2$ and CH_4 between 1850 and 4000Å. J.Geophys. Res. 68, 6431-6439.

U.S. Standard Atmosphere Supplements, 1966: U.S. Government Printing Office, Washington, D.C. 20403, 289p.

Vanderslice,J.T.,E.A.Mason and W.G.Maisch,1960: Interactions between ground state oxygen atoms and molecules: O-O and O_2-O_2. J.Chem Phys.,32,515-524.

Volman,D.H., 1956a: Photochemical evidence related to the excited states of oxygen. J.Chem. Phys.,24,122-124.

Volman,D.H.,1956b : Photochemical oxygen-hydrogen reaction at 1849 Å. J Chem. Phys., 25,288-292.

Washida,N.,Y.Mori and I.Tanaka, 1971: Quantum yield of ozone formation from photolysis of the oxygen molecule at 1849 and 1931 Å. J.Chem.Phys.,54, 1119-1122.

Watanabe, K, 1958: Ultraviolet absorption processes in the upper atmosphere. Adv. in Geophys., 5, 153-221.

Watanabe,K.,E.C.Y. Inn and M. Zelikoff, 1953: Absorption coefficients of oxygen in the vacuum ultraviolet. J.Chem. Phys.,21,1026-1030.

Widing,K.G.,J.D.Purcell and G.D.Sandlin, 1970: The UV continuum 1450-2100Å and the problem of the solar temperature minimum. Solar Physics.,12,52-62.

Wilkinson,P.G. and R.S.Mulliken, 1957: Dissociation processes in oxygen above 1750 A. Astrophys. J., 125,594-600.

Wu,M.F., 1973: Observation and analysis of trace constituents in the stratosphere. Annual report prepared for Dept. of Transportation, CIAP program under contract DOT-OS-20217, by Environmental Research & Technology,INC. 427 Marrett Road, Lexington,Massachusetts,02173, 218p.

Figures

Fig. 1 Potential curves for the oxygen molecule. Potential energy V(eV) is relative to the bottom of the potential curve for the $X^3\Sigma_g^-$ state. r(Å) is the inter nuclear distance.

Fig. 2 Solar spectral irradiance outside the earth's atmosphere. Thin solid curves show the black-body spectra at a given temperature.

Fig. 3 Variations of the solar ultraviolet flux during a solar cycle. Data of the solar flux at 1750Å are taken from: A,Detwiler et al.(1961); B,Brewer and Wilson(1965); C,Widing et al.(1970); D,Heath(1973); E,Prag and Morse (1970); F,Parkinson and Reeves (1969); G,Brueckner and Moe (1972); H,Nishi et al. (1973). Data shown by filled circles are obtained by photographic techniqe and those shown by filled squares are by photoelectric technique.

Fig.4 Absorption cross section of the oxygen molecule in the region 1450 to 2500Å. The absorption in the Schumann-Runge continuum (1350-1750A) and the Schumann-Runge bands (1750-2000Å) corresponds to the transition $O_2(X^3\Sigma_g^-) \rightarrow O_2(B^3\Sigma_u^-)$, and the Herzberg continuum (2000-2454Å) is caused from the forbidden transition, $O_2(X^3\Sigma_g^-) \rightarrow O_2(A^3\Sigma_u^+)$.

Fig. 5 The rotational structure of the Schumann-Runge bands around 1810A at 250 K. Line positions and strengths are shown schematically. Intensity scale (arbitrary unit) in the upper part (v'-1 progression) is exaggerated by a factor of 4×10^3 compared to the lower part (v'-0 progression).

Fig. 6 Shape of an absorption line and definitions of the half-width and the half half-width.

Fig. 7 Integrated band absorption coefficient K(v',v'') of the Schumann-Runge bands for v'' = 0 .

△ Ditchburn and Heddle(1954) Exp. ; ▲—▲ Bethke(1959b)Exp ;

○ Jarmain(1963) Cal ; ▽ Halmann(1966) Exp ;

■---■ Farmer et al. (1968) Exp ;

+ Halmann and Laulicht(1960) Cal ; ◇ Ory and Gittleman(1964)Cal;

× Harris et al.(1969) Cal ; ^ Murrell and Taylor(1969) Cal ;

+ Allison et al.(1971) Cal .

Notation Exp means the experimental value and Cal means the theoretically calculated value.

Fig. 8 Integrated band absorption coefficient $K(v',v'')$ of the Schumann-Runge bands for $v''=1$.

△ Hudson and Carter(1968) Exp ;

Ory and Gittleman(1964) Cal ; ⧺ Halmann and Laulicht(1966)Cal ;

× — × Harris et al.(1969) Cal ; + Allison et al. (1971) Cal.

Notations Exp and Cal have the same meaning as in Fig. 7.

Fig. 9 Intensity distribution of the rotational lines in 15 wavelength intervals. The indicated values on the ordinate scale apply to the interval 1 only. The other intervals are displaced upward a distance corresponding to 10. The short horizontal lines show the ordinate for each curve corresponding to the value 20.

Fig.10 Schematic diagram of the cumulative probability of lines, S_{cum}, for various distribution functions.

Fig.11 Effect of the predissociation on the photodissociation rate of the oxygen molecule. Solid curves show the dissociation rate including predissociation, and the broken curves without predissociation.

Fig.12 The ratio of dissociation rate including the predissociation to that excluding it.

Fig.13 Effect of the solar radiation $F_\nu(\infty)$ on the photodissociation rate of the molecular oxygen. For each curve ,assumed Cases for $F_\nu(\infty)$, $p(S)$, $\bar{k}$, $\bar{d}$, and $\bar{\alpha}$ are shown as a Table in the Figure.

Fig.14 Effect of the distribution function of line intensities on the photodissociation rate of the oxygen molecule for three Cases of the solar radiation, $F_\nu(\infty)$: Case A, Case B , and Case C.

Fig.15 Effect of the mean absorption coefficient $\bar{k}$ on the photodissociation rate of the oxygen molecule for two cases of the solar radiation $F_\nu(\infty)$; Case B, and Case C.

Fig.16 Effect of the mean line spacing $\bar{d}$ on the photodissociation rate of the oxygen molecule for two cases of the solar radiation $F_\nu(\infty)$; Case B and Case C.

Fig.17 Effect of the mean line half-width $\bar{\alpha}$ on the photodissociation rate of the oxygen molecule for two cases of the solar radiation $F_\nu(\infty)$; Case B and Case C.

Fig.18 Comparison of the dissociation rate of oxygen molecule obtained by various methods. Our results by the band model approximation are shown for the most appropriate cases of p(S), $\bar{d}$ and $\bar{\alpha}$.

Fig.19 Average band-absorption coefficients of the oxygen molecule adopted to calculate the dissociation rate. Curve (3) is equal to the $\bar{k}$ of Case A adopted in the band model.

Fig.20 Dissociation rate of the oxygen molecule deduced from the average band-absorption coefficients shown in Fig. 19, and that from the band model.

Fig.21 Vertical profiles of ozone calculated for the atmosphere of 30°N lat winter (pure oxygen atmosphere model). Two dotted curves show the range of observations.

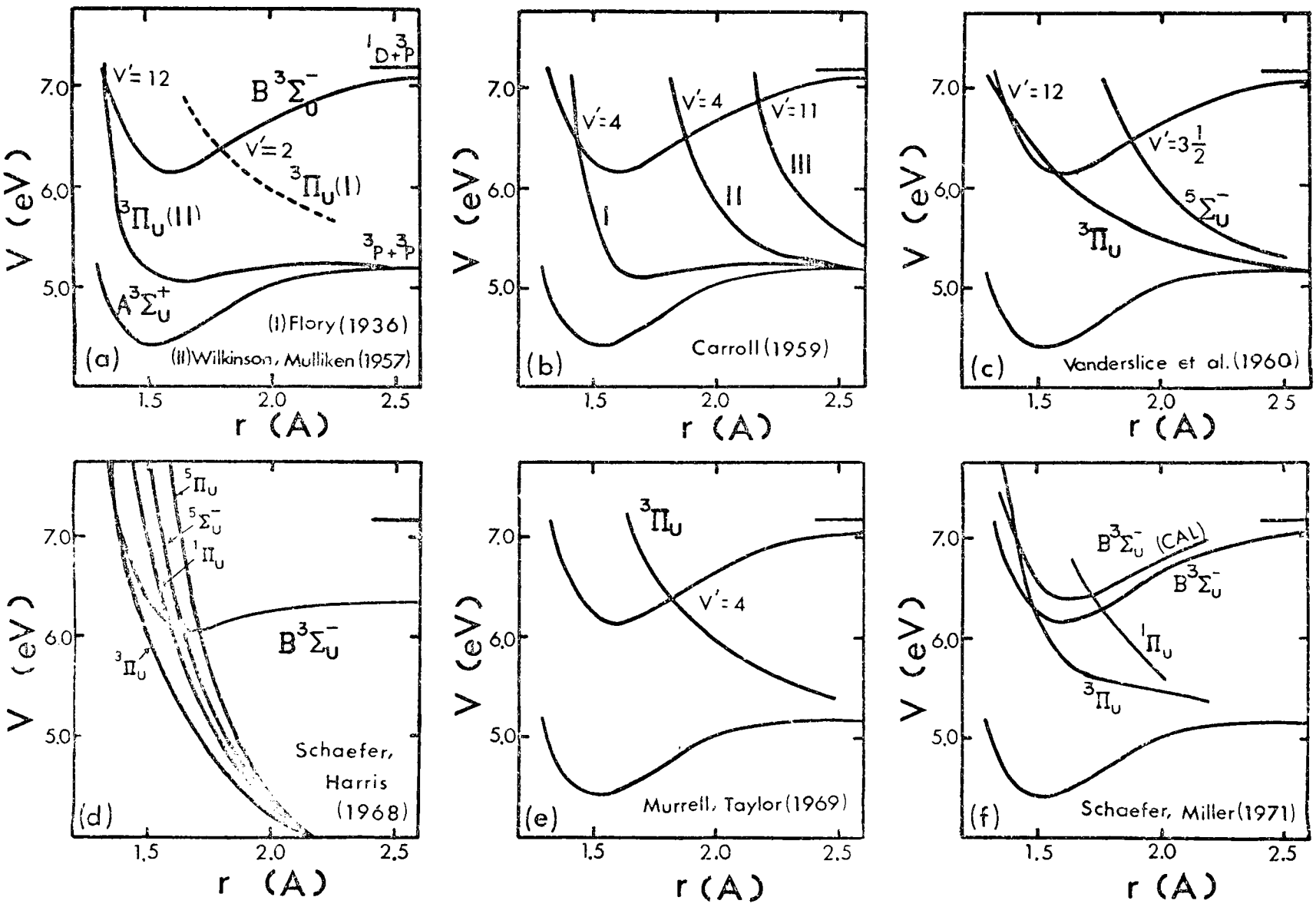
V (eV)
r (A)
7.0
6.0
5.0
1.5
2.0
2.5
(a)
V'=12
V'=2
B 3Σ-u
3Πu(I)
3Πu(II)
A 3Σ+u
1D+3P
3P+3P
(I) Flory (1936)
(II) Wilkinson, Mulliken (1957)
(b)
V'=4
V'=4
V'=11
I
II
III
Carroll (1959)
(c)
V'=12
V'=3 1/2
5Σ-u
3Πu
Vanderslice et al. (1960)
(d)
5Πu
5Σ-u
1Πu
3Πu
B 3Σ-u
Schaefer, Harris (1968)
(e)
3Πu
V'=4
Murrell, Taylor (1969)
(f)
B 3Σ-u (CAL)
B 3Σ-u
1Πu
3Πu
Schaefer, Miller (1971)

Fig. 1

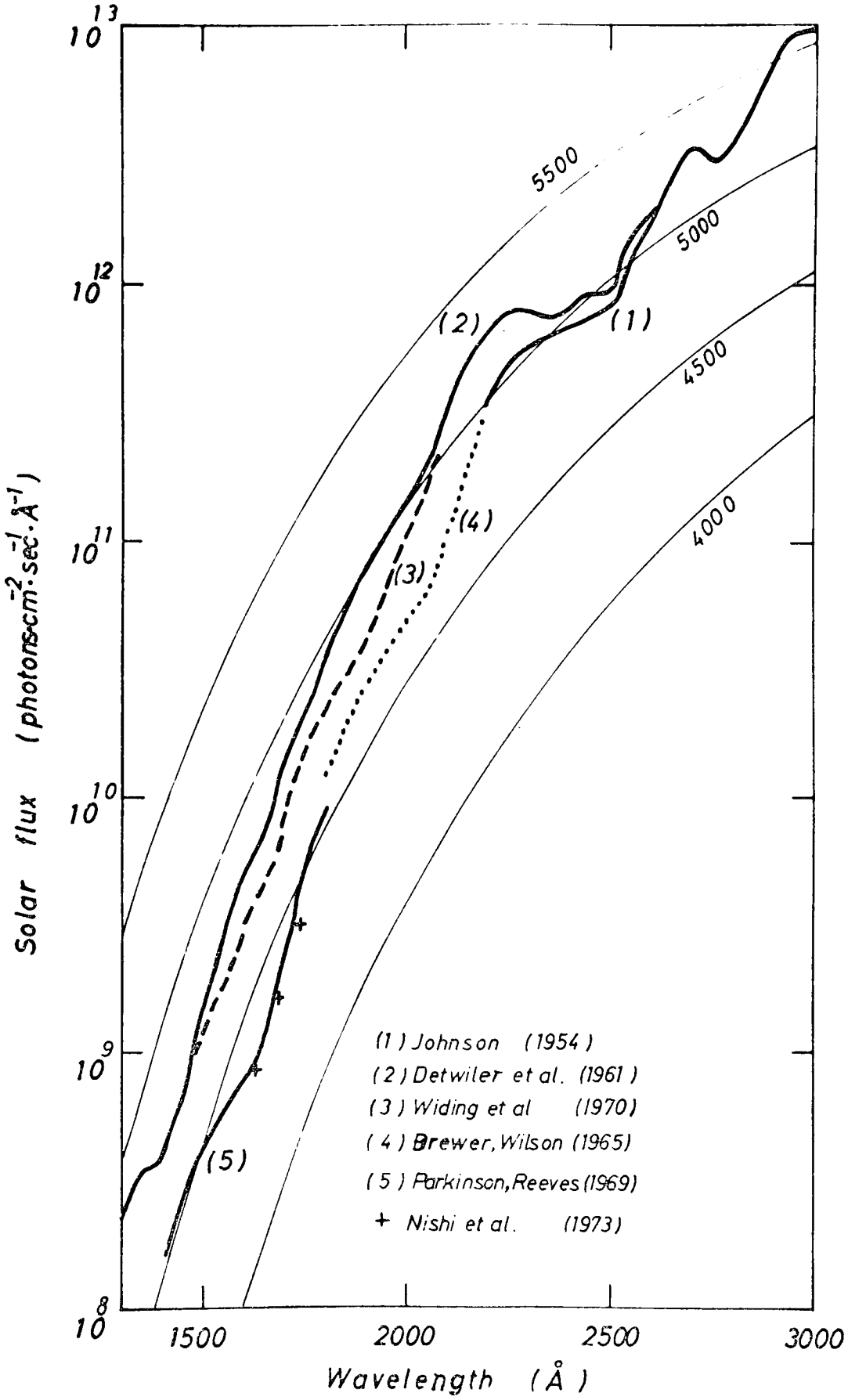
Solar flux (photons·cm⁻²·sec⁻¹·Å⁻¹)
Wavelength (Å)
10^13
10^12
10^11
10^10
10^9
10^8
1500
2000
2500
3000
5500
5000
4500
4000
(1)
(2)
(3)
(4)
(5)
(1) Johnson (1954)
(2) Detwiler et al. (1961)
(3) Widing et al (1970)
(4) Brewer, Wilson (1965)
(5) Parkinson, Reeves (1969)
+ Nishi et al. (1973)

Fig. 2

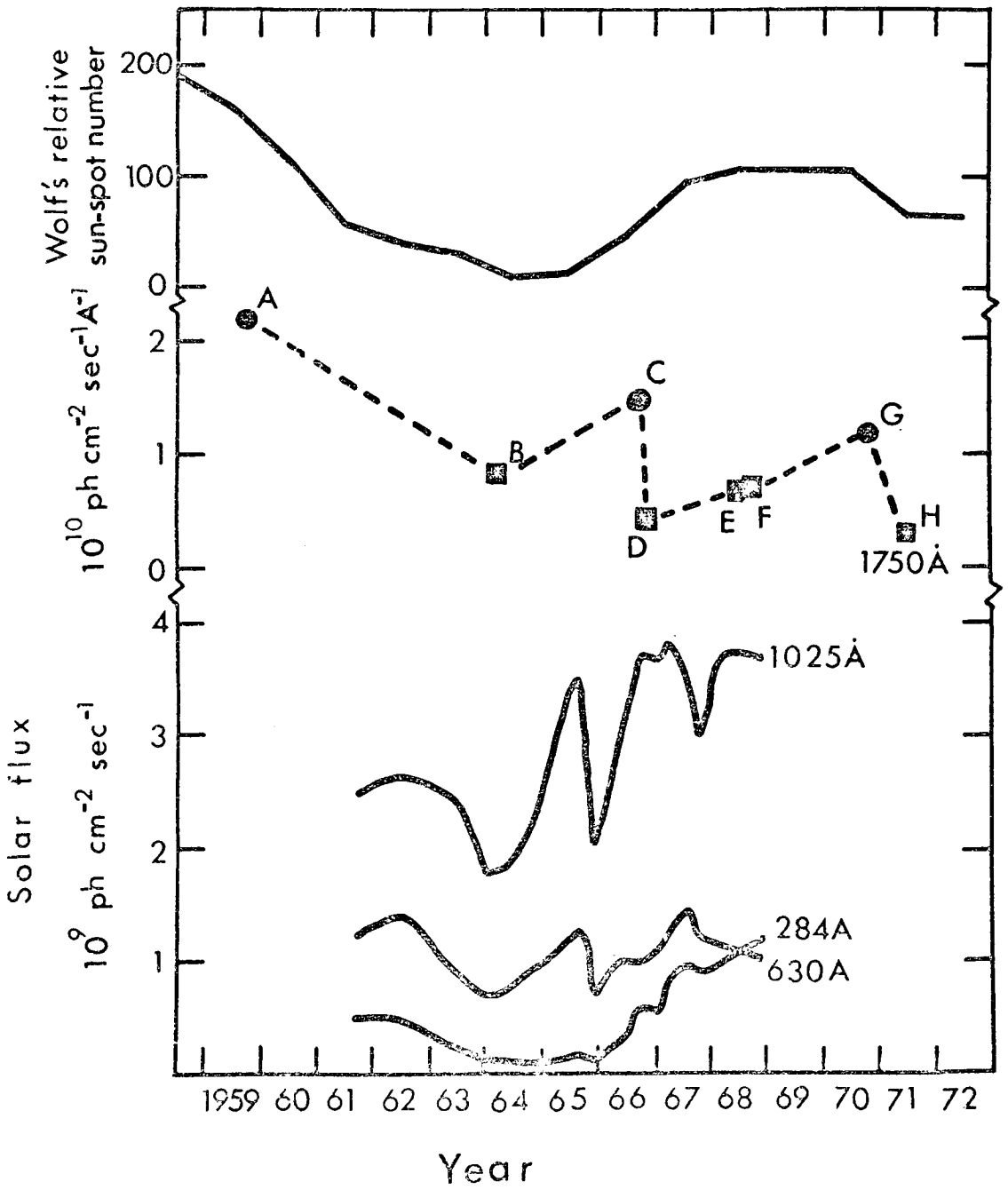
Wolf's relative sun-spot number
200
100
0
10^{10} ph cm^{-2} $sec^{-1}A^{-1}$
2
1
0
A
B
C
D
E
F
G
H
1750Å
Solar flux
10^{9} ph cm^{-2} sec^{-1}
4
3
2
1
1025Å
284A
630A
1959 60 61 62 63 64 65 66 67 68 69 70 71 72
Year

Fig. 3

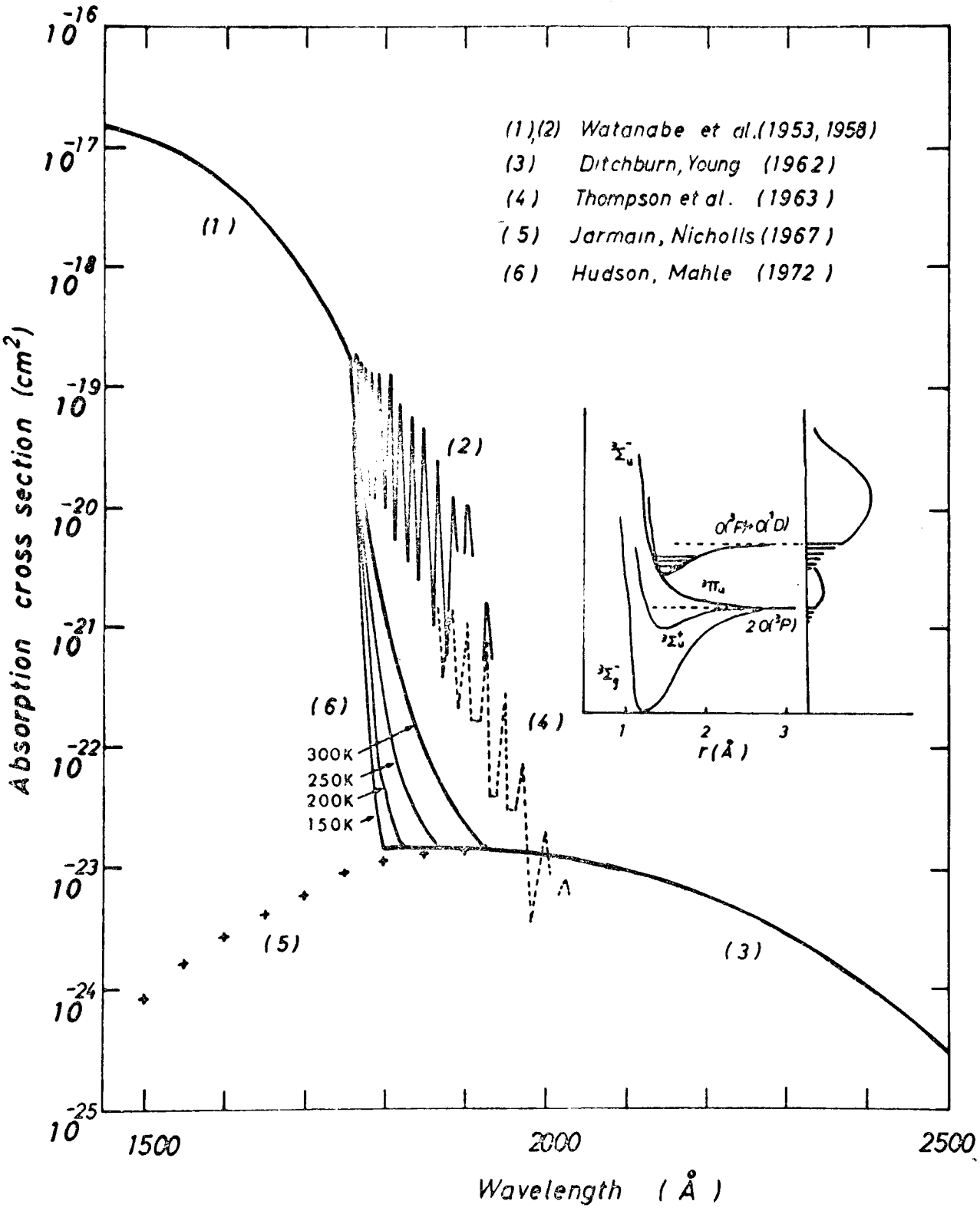
(1),(2) Watanabe et al.(1953, 1958)
(3) Ditchburn, Young (1962)
(4) Thompson et al. (1963)
(5) Jarmain, Nicholls (1967)
(6) Hudson, Mahle (1972)
(1)
(2)
(3)
(4)
(5)
(6)
300K
250K
200K
150K
A
a^3F+a^3D
$2a^3P$
r(Å)
Absorption cross section (cm^2)
Wavelength (Å)
1500
2000
2500

Fig. 4

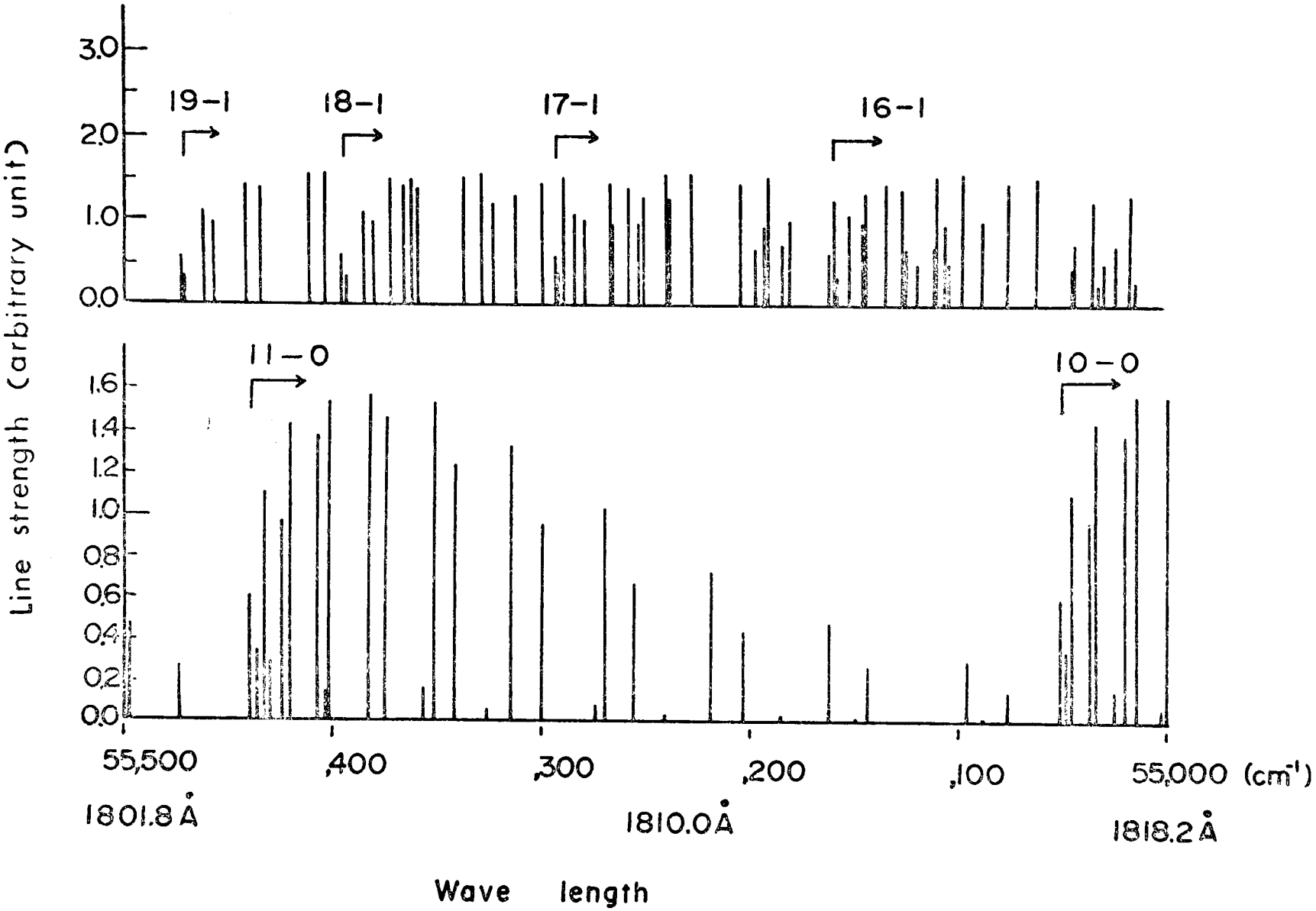
Line strength (arbitrary unit)
3.0
2.0
1.0
0.0
19-1
18-1
17-1
16-1
11-0
10-0
1.6
1.4
1.2
1.0
0.8
0.6
0.4
0.2
0.0
55,500
,400
,300
,200
,100
55,000 (cm⁻¹)
1801.8 Å
1810.0 Å
1818.2 Å
Wave length

Fig. 5

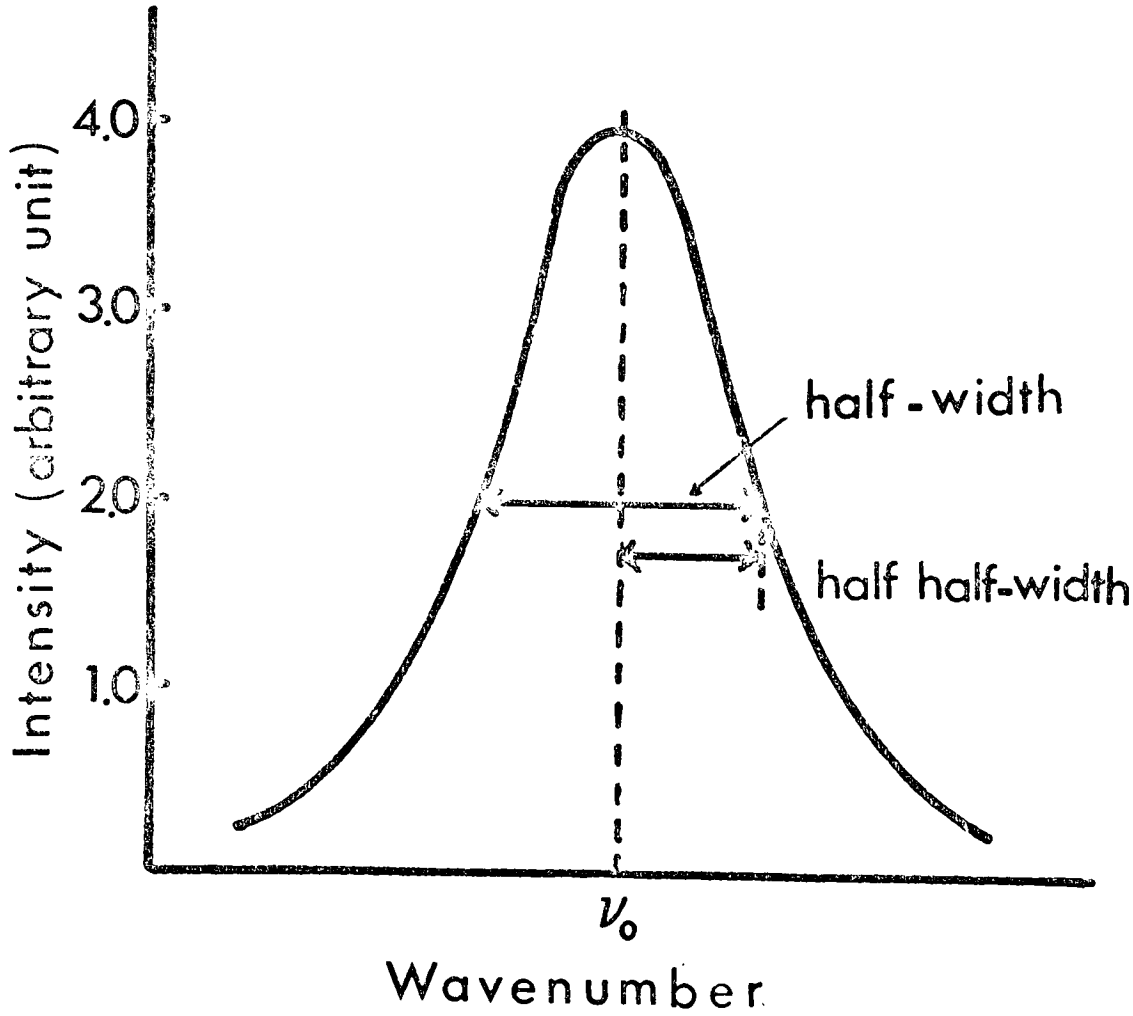
Intensity (arbitrary unit)
4.0
3.0
2.0
1.0
half - width
half half-width
ν_0
Wavenumber

Fig. 6

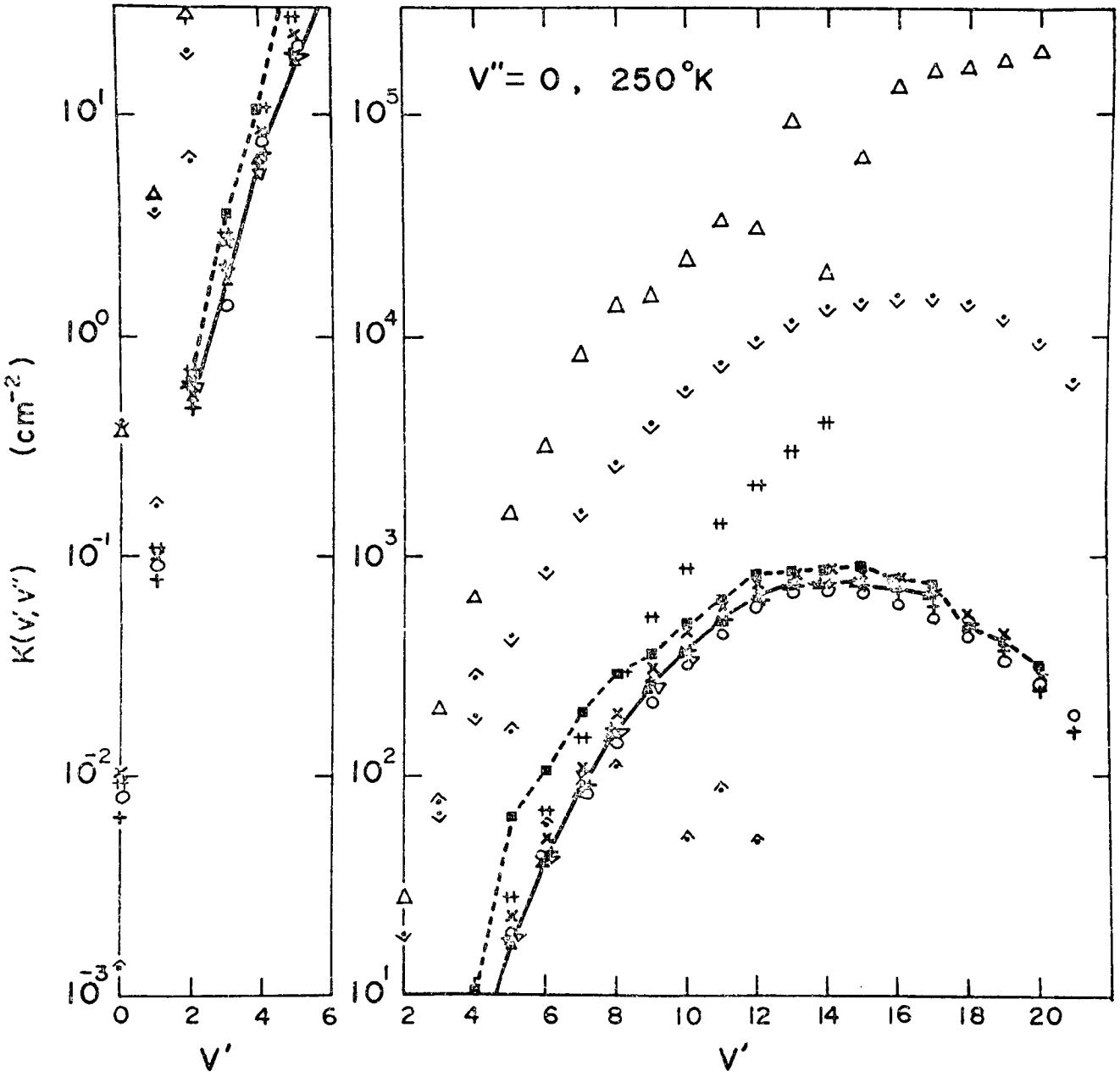

Fig. 7

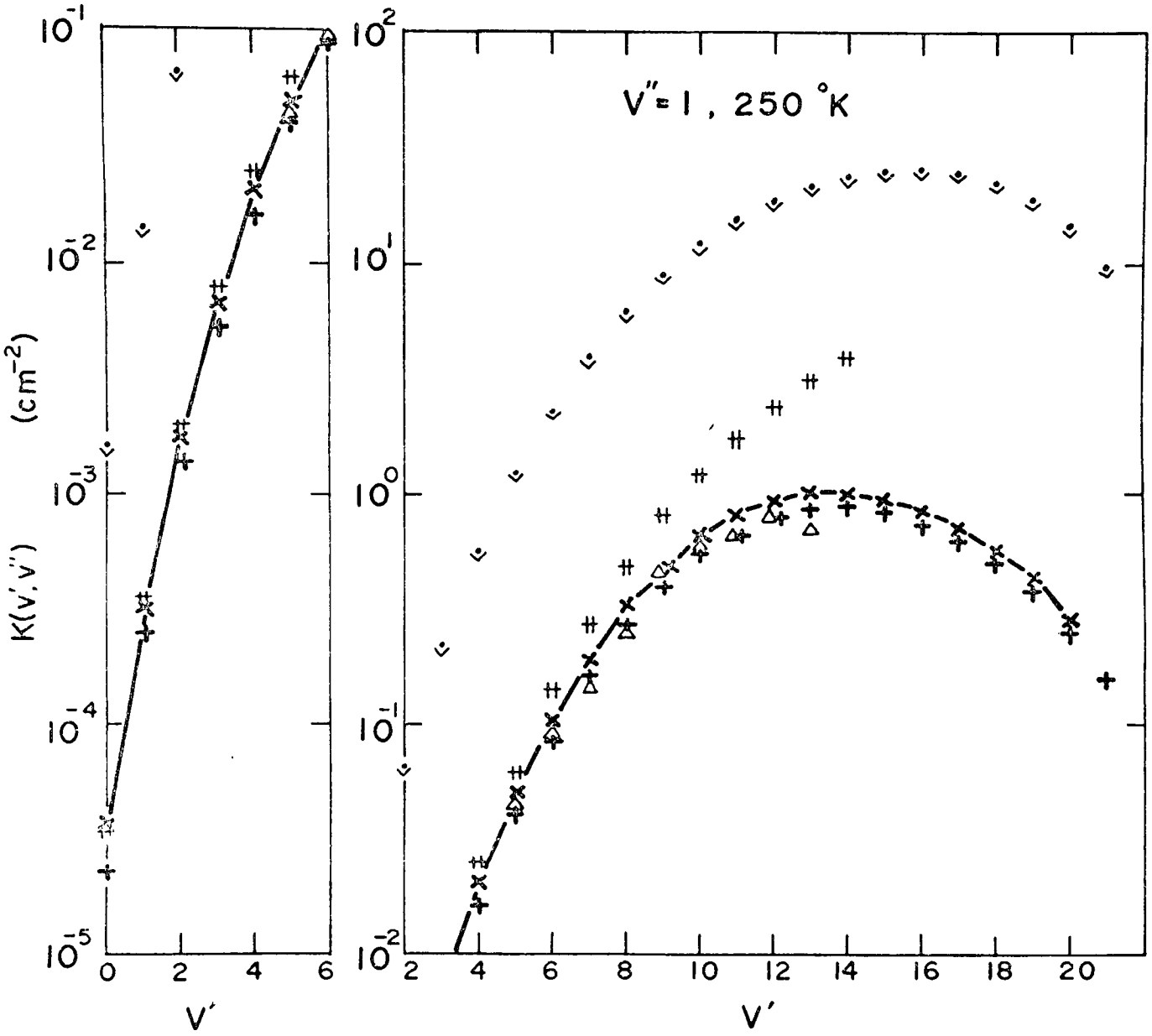

Fig. 8

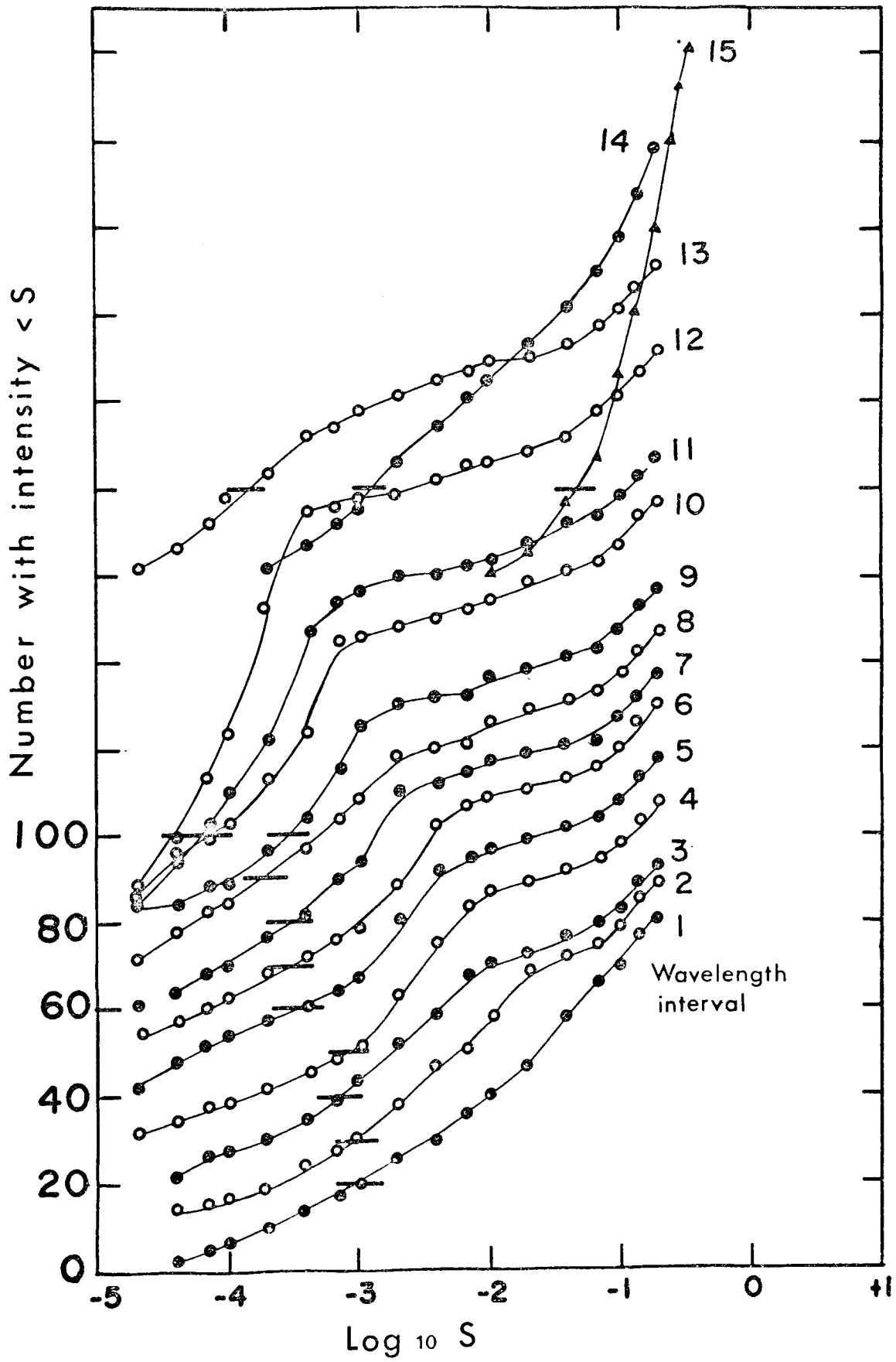
Number with intensity < S
100
80
60
40
20
0
-5
-4
-3
-2
-1
0
+1
Log 10 S
15
14
13
12
11
10
9
8
7
6
5
4
3
2
1
Wavelength interval

Fig. 9

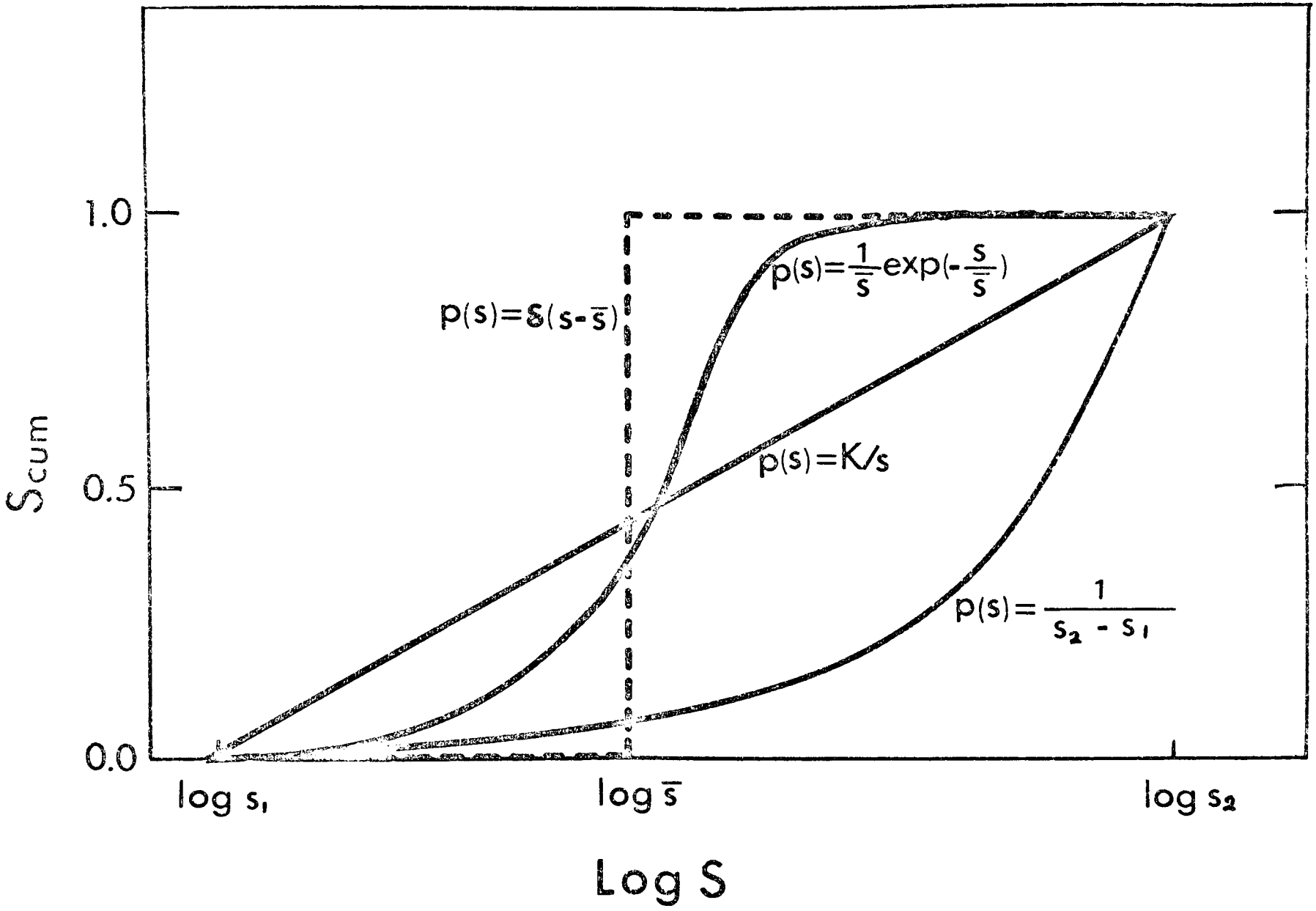
1.0
0.5
0.0
S_{cum}
$p(s)=\delta(s-\bar{s})$
$p(s)=\frac{1}{\bar{s}}\exp(-\frac{s}{\bar{s}})$
$p(s)=K/s$
$p(s)=\frac{1}{s_2-s_1}$
log s_1
log $\bar{s}$
log s_2
Log S

Fig. 10

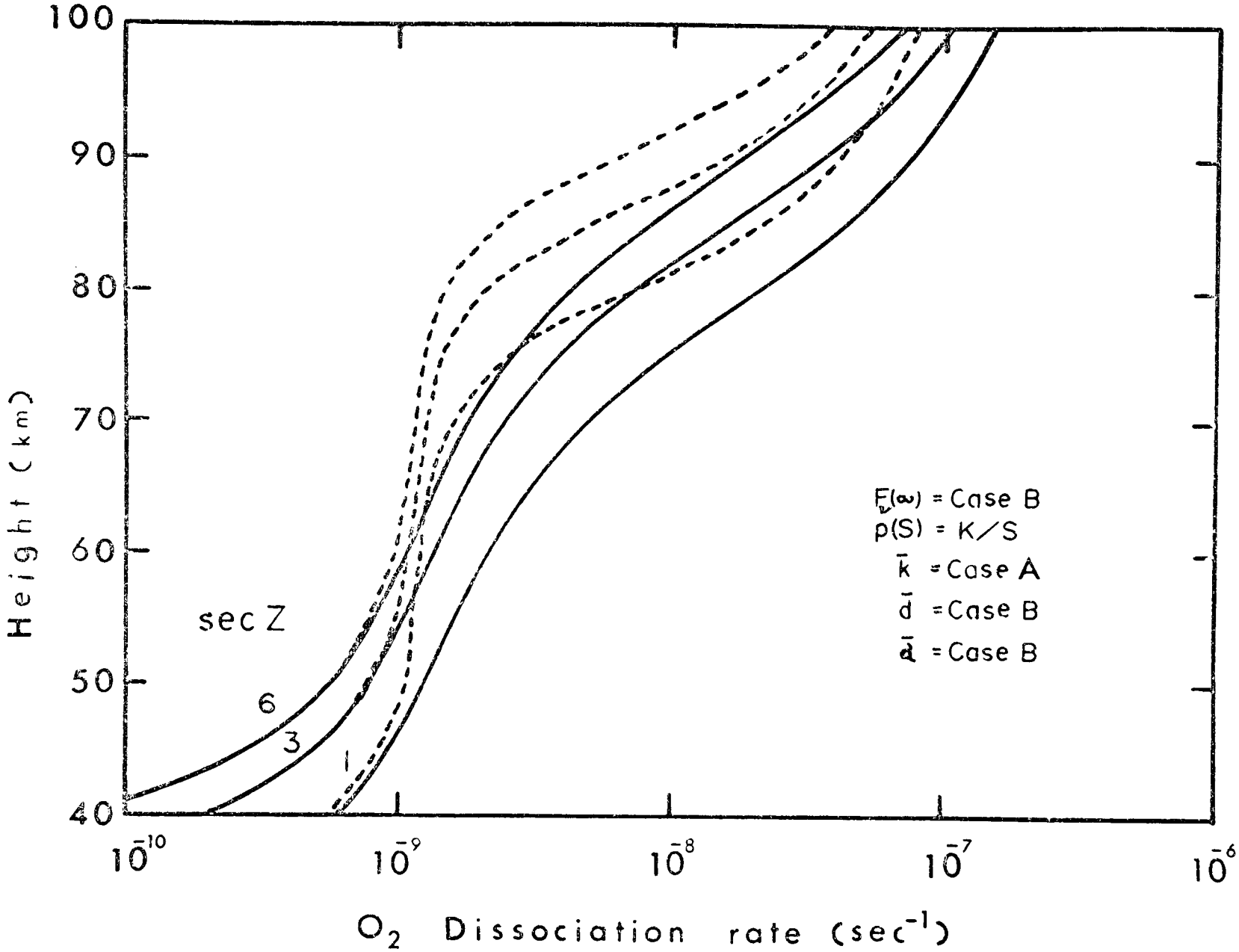
100
90
80
70
60
50
40
Height (km)
sec Z
6
3
1
$F_\nu(\infty)$ = Case B
p(S) = K/S
$\bar{k}$ = Case A
$\bar{d}$ = Case B
$\bar{d}$ = Case B
10^{-10}
10^{-9}
10^{-8}
10^{-7}
10^{-6}
O_2 Dissociation rate (sec^{-1})

Fig. 11

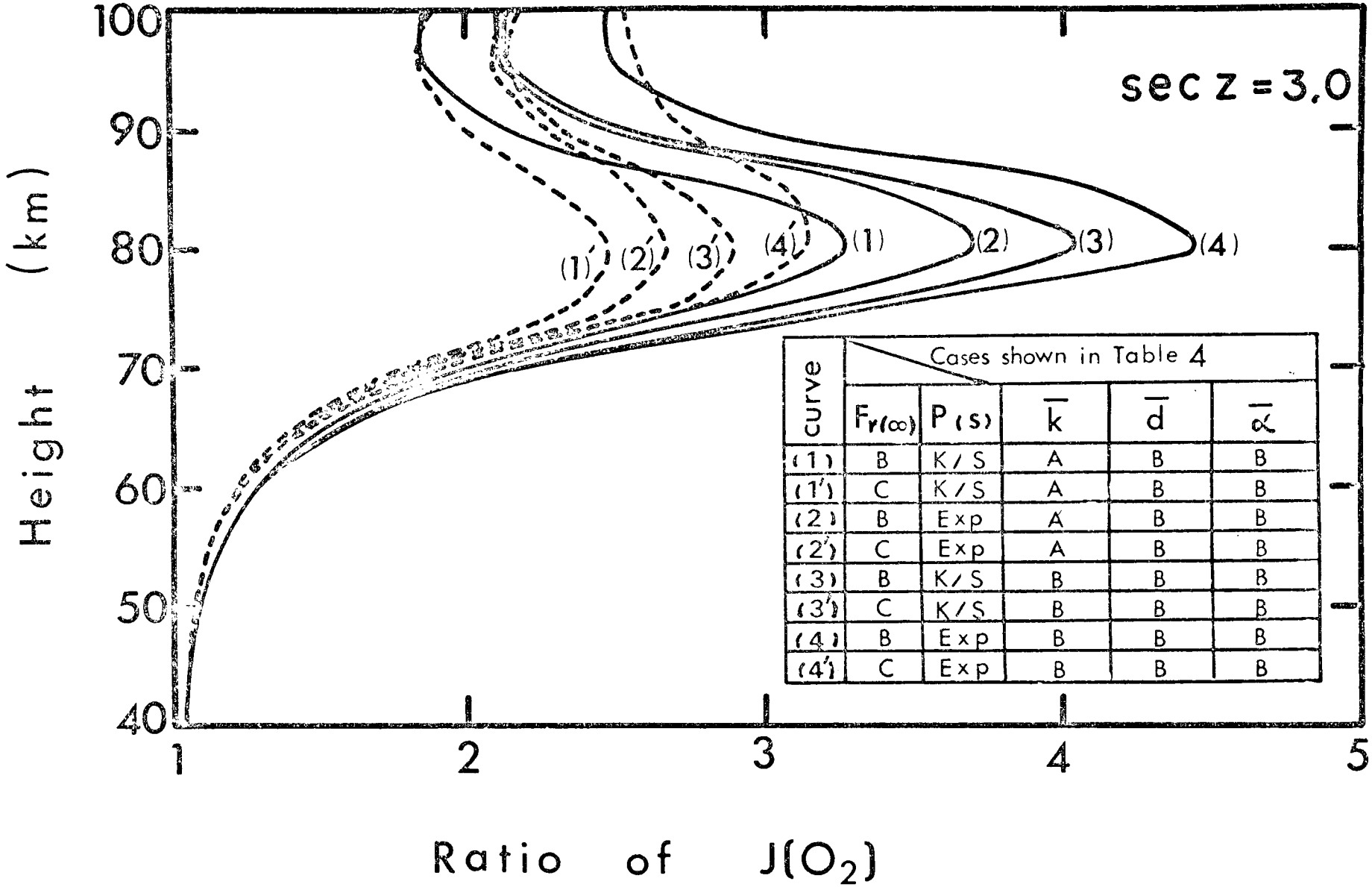

curve	Cases shown in Table 4				
	$F_{r(\infty)}$	P(s)	$\bar{k}$	$\bar{d}$	$\bar{\alpha}$
(1)	B	K/S	A	B	B
(1')	C	K/S	A	B	B
(2)	B	Exp	A	B	B
(2')	C	Exp	A	B	B
(3)	B	K/S	B	B	B
(3')	C	K/S	B	B	B
(4)	B	Exp	B	B	B
(4')	C	Exp	B	B	B

Fig. 12

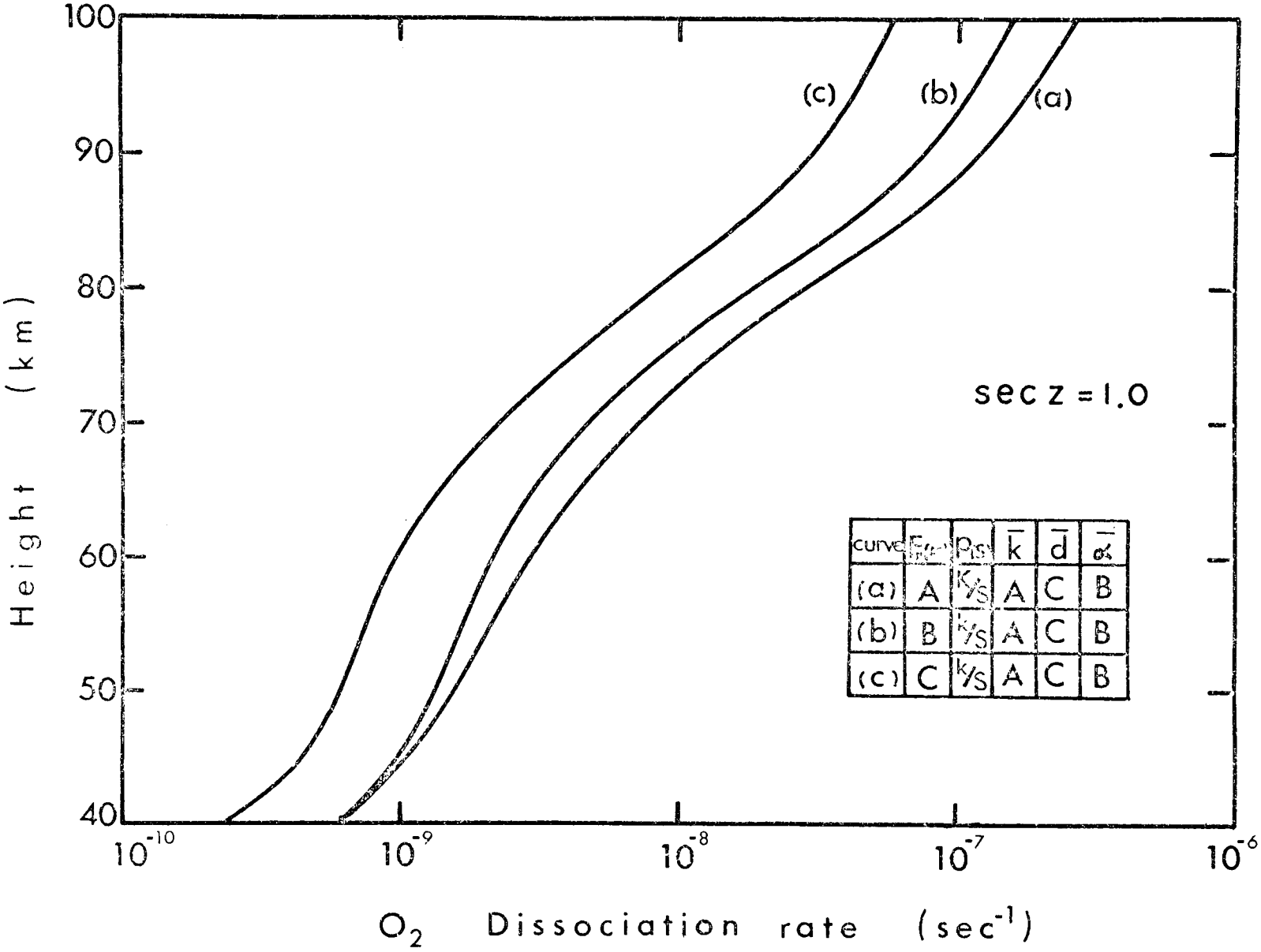
100
90
80
70
60
50
40
Height (km)
(c)
(b)
(a)
sec z = 1.0
curve
(a) A K/S A C B
(b) B K/S A C B
(c) C K/S A C B
10^{-10}
10^{-9}
10^{-8}
10^{-7}
10^{-6}
O_2 Dissociation rate (sec^{-1})

Fig. 13

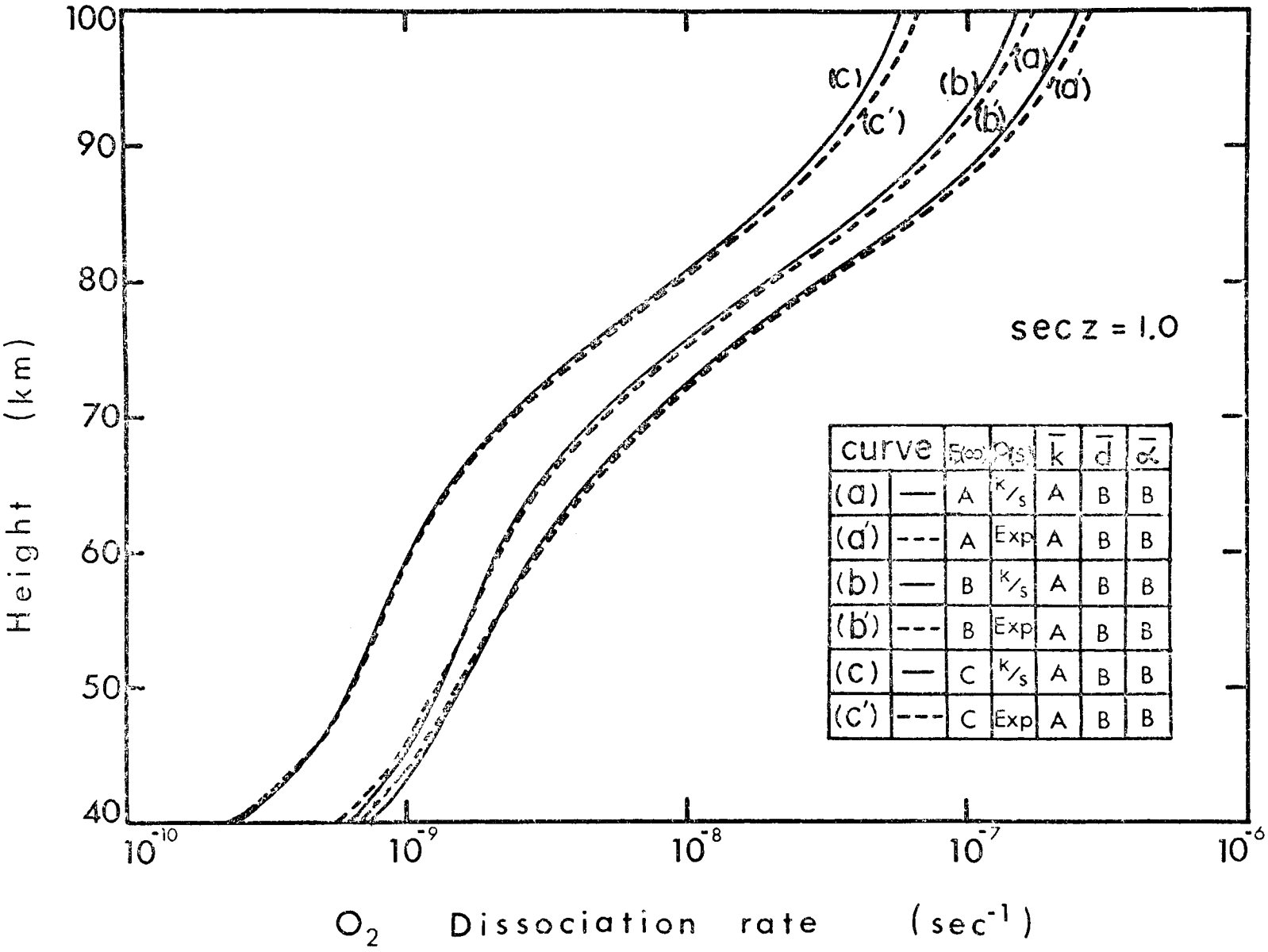
100
90
80
70
60
50
40
Height (km)
(c)
(c')
(b)
(b')
(a)
(a')
sec z = 1.0
curve | $S(\infty)$ | $P_{1/2}$ | $\bar{k}$ | $\bar{d}$ | $\bar{\alpha}$
(a) — A K/S A B B
(a') --- A Exp A B B
(b) — B K/S A B B
(b') --- B Exp A B B
(c) — C K/S A B B
(c') --- C Exp A B B
10^{-10}
10^{-9}
10^{-8}
10^{-7}
10^{-6}
O_2 Dissociation rate (sec^{-1})

Fig. 14

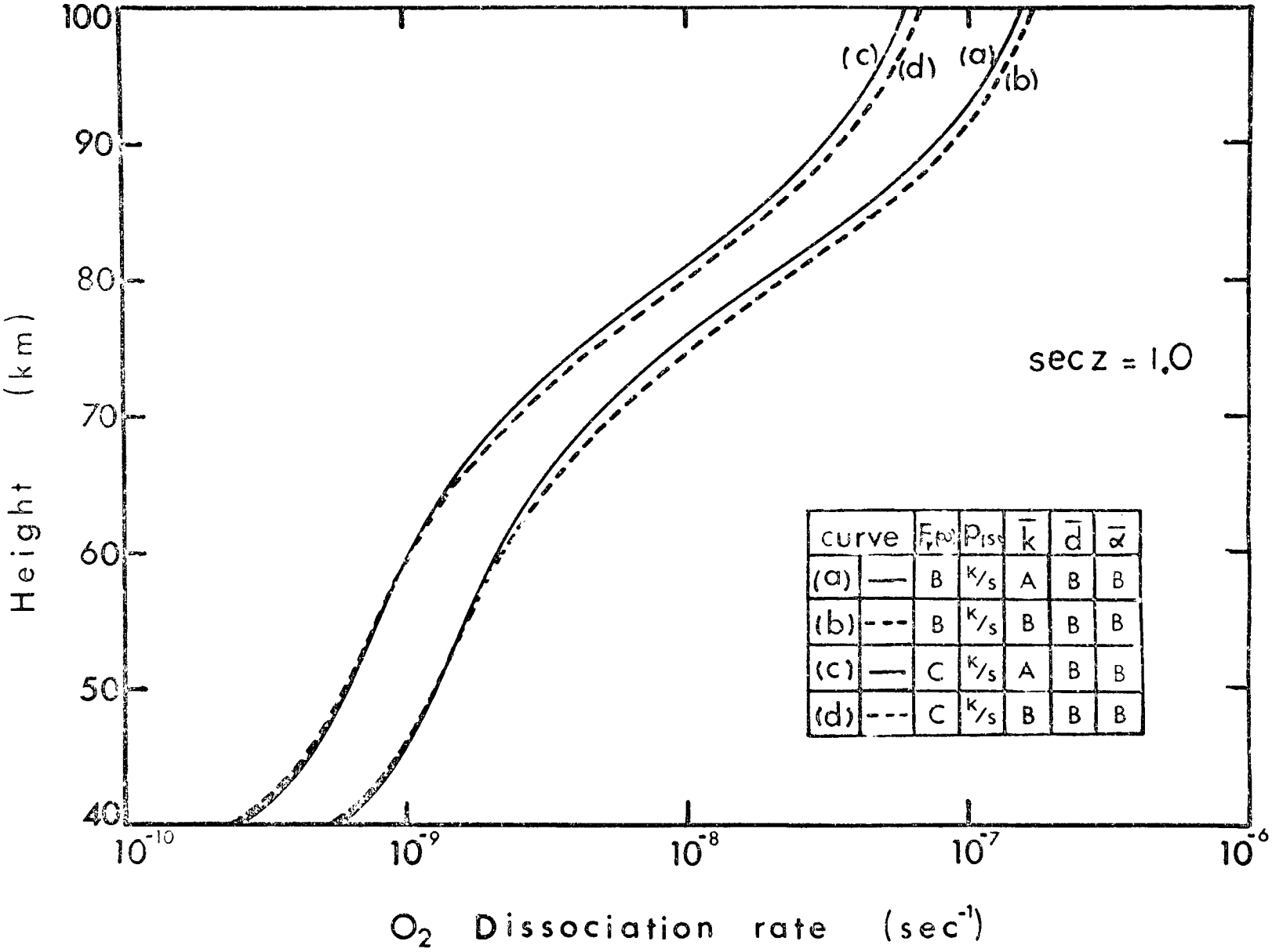
100
90
80
70
60
50
40
Height (km)
(c)
(d)
(a)
(b)
sec z = 1.0
curve
B
C
K/s
A
B
10^{-10}
10^{-9}
10^{-8}
10^{-7}
10^{-6}
O_2 Dissociation rate (sec^{-1})

Fig. 15

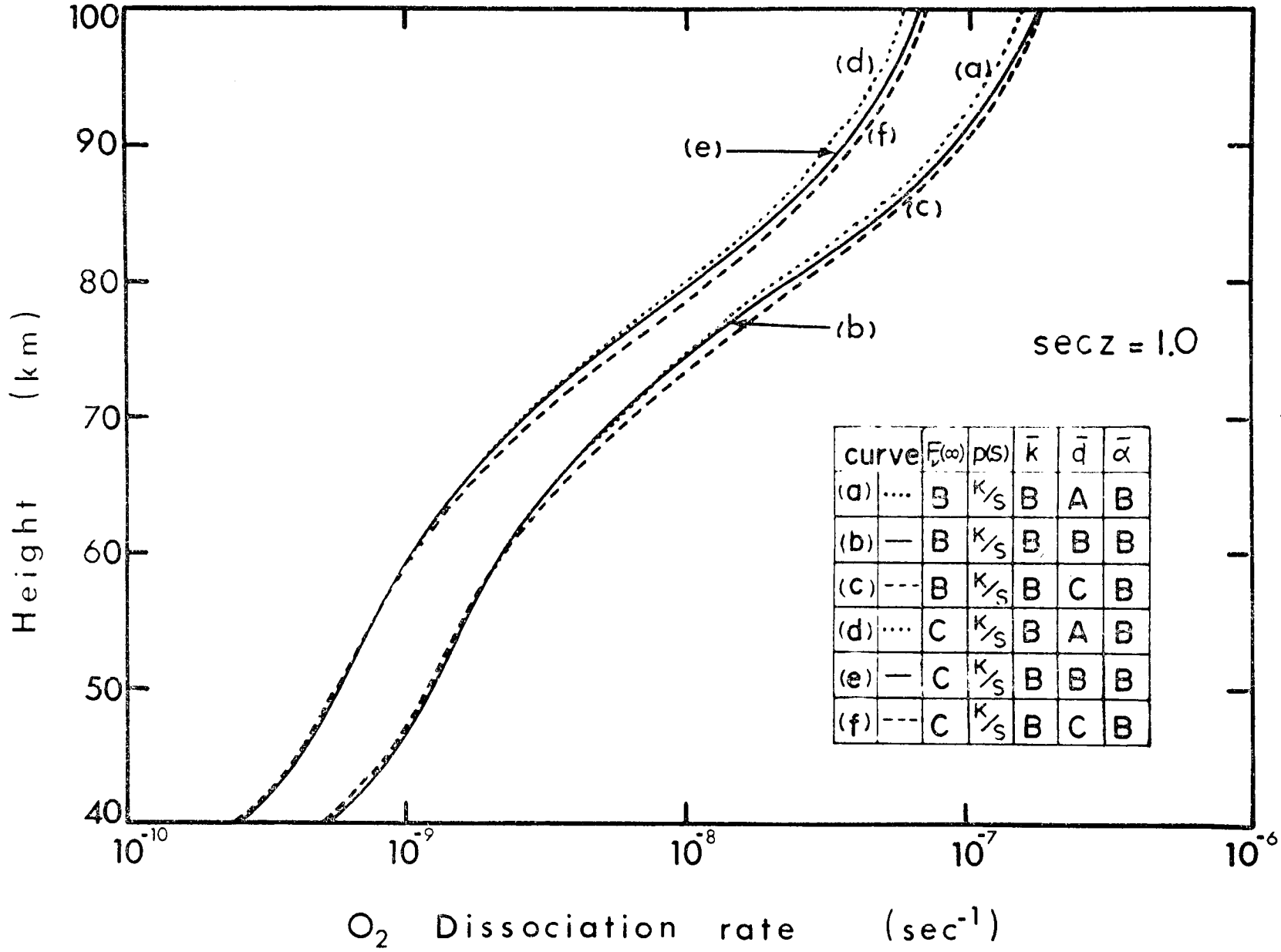
100
90
80
70
60
50
40
Height (km)
(d)
(a)
(e)
(f)
(c)
(b)
secz = 1.0
curve | F(∞) | p(s) | k̄ | d̄ | ᾱ
(a) .... B K/S B A B
(b) — B K/S B B B
(c) --- B K/S B C B
(d) .... C K/S B A B
(e) — C K/S B B B
(f) --- C K/S B C B
10^{-10}
10^{-9}
10^{-8}
10^{-7}
10^{-6}
O_2 Dissociation rate (sec^{-1})

Fig. 16

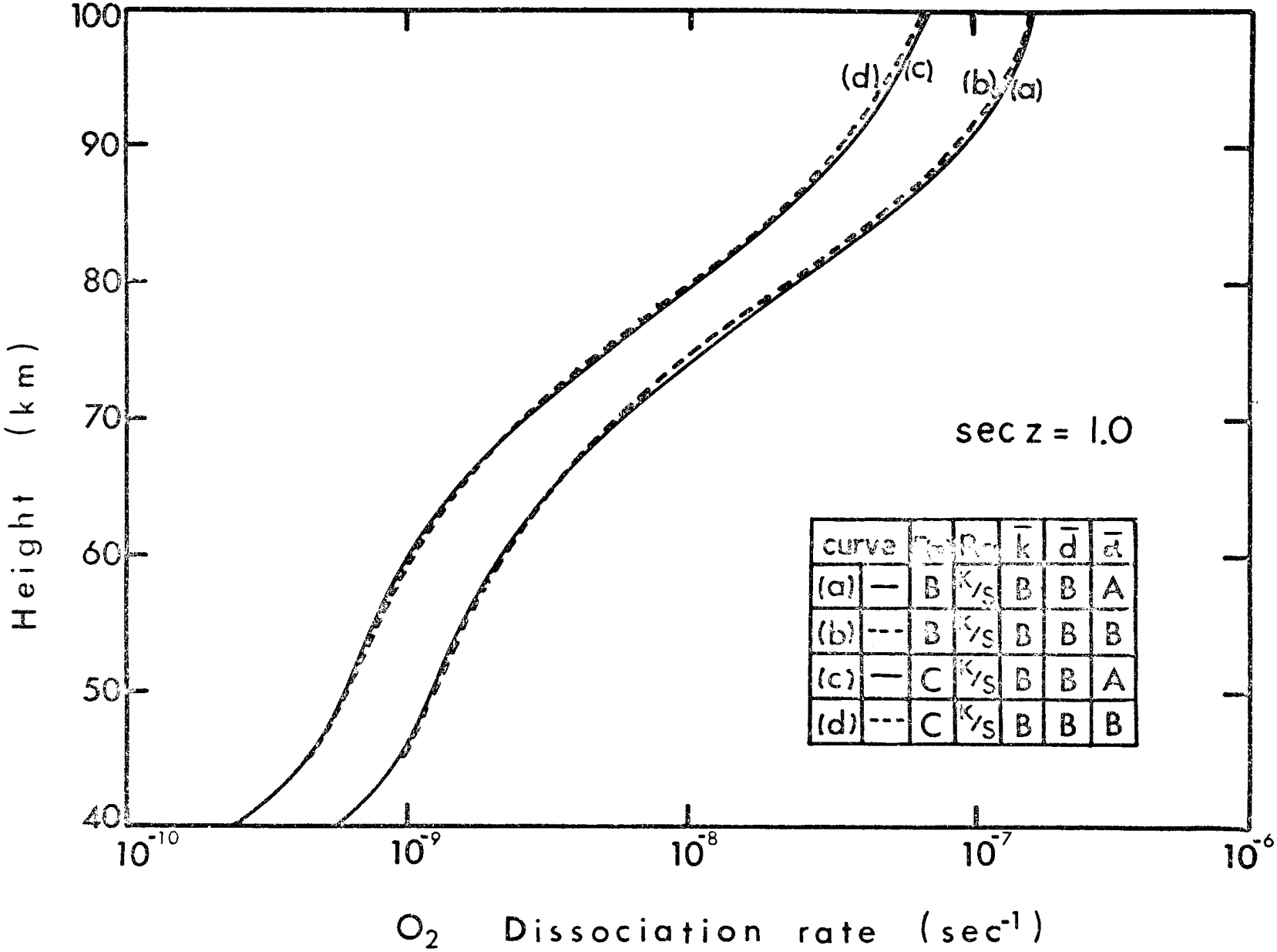
100
90
80
70
60
50
40
Height (km)
(d)
(c)
(b)
(a)
sec z = 1.0
curve
$\bar{k}$
$\bar{d}$
$\bar{a}$
(a) — B K/S B B A
(b) --- B K/S B B B
(c) — C K/S B B A
(d) --- C K/S B B B
10^{-10}
10^{-9}
10^{-8}
10^{-7}
10^{-6}
O_2 Dissociation rate (sec^{-1})

Fig. 17

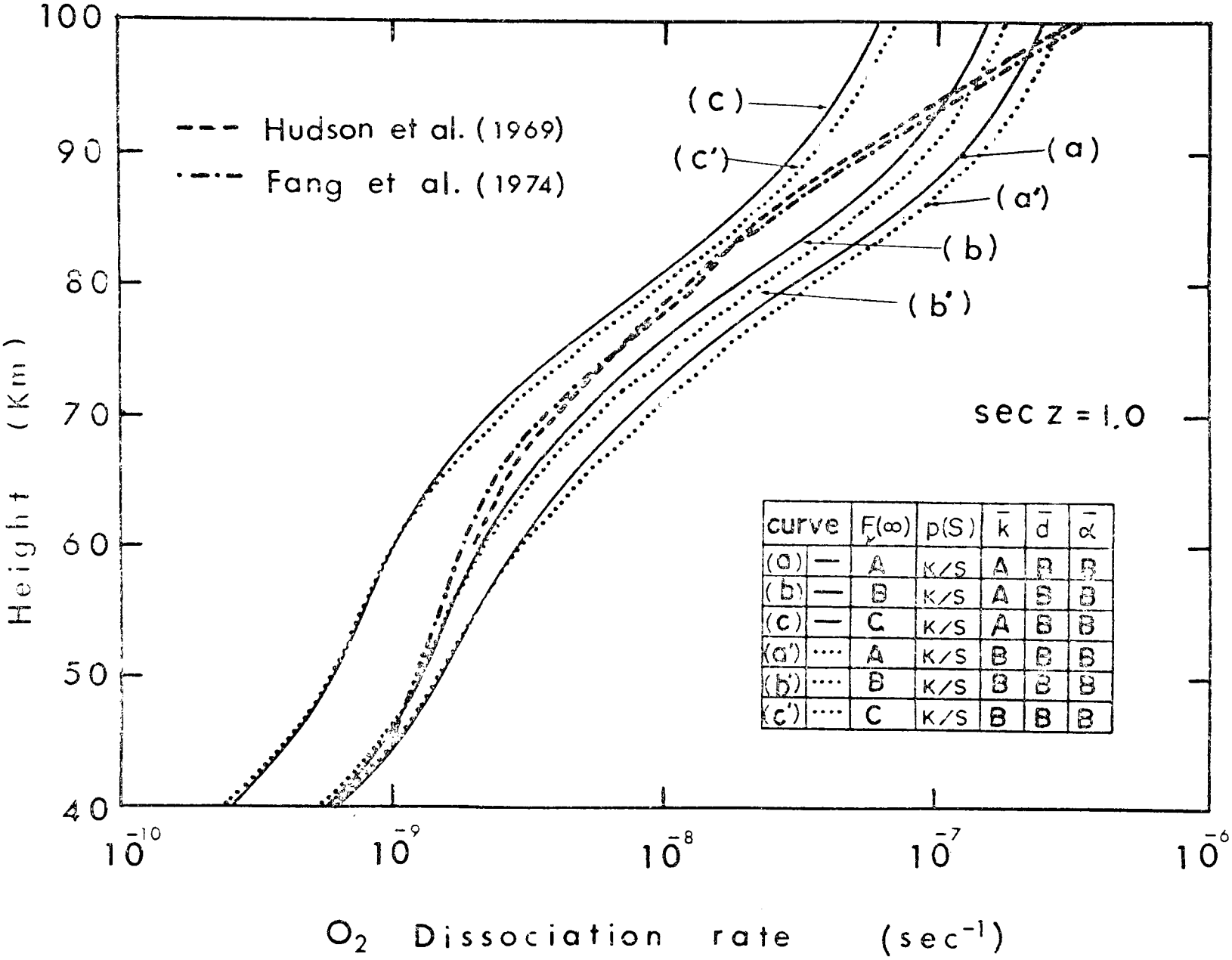
100
90
80
70
60
50
40
Height (Km)
Hudson et al. (1969)
Fang et al. (1974)
(c)
(c')
(a)
(a')
(b)
(b')
sec z = 1.0
curve | F(∞) | p(S) | k̄ | d̄ | ᾱ
(a) — | A | K/S | A | B | B
(b) — | B | K/S | A | B | B
(c) — | C | K/S | A | B | B
(a') ···· | A | K/S | B | B | B
(b') ···· | B | K/S | B | B | B
(c') ···· | C | K/S | B | B | B
10^{-10}
10^{-9}
10^{-8}
10^{-7}
10^{-6}
O_2 Dissociation rate (sec^{-1})

Fig. 18

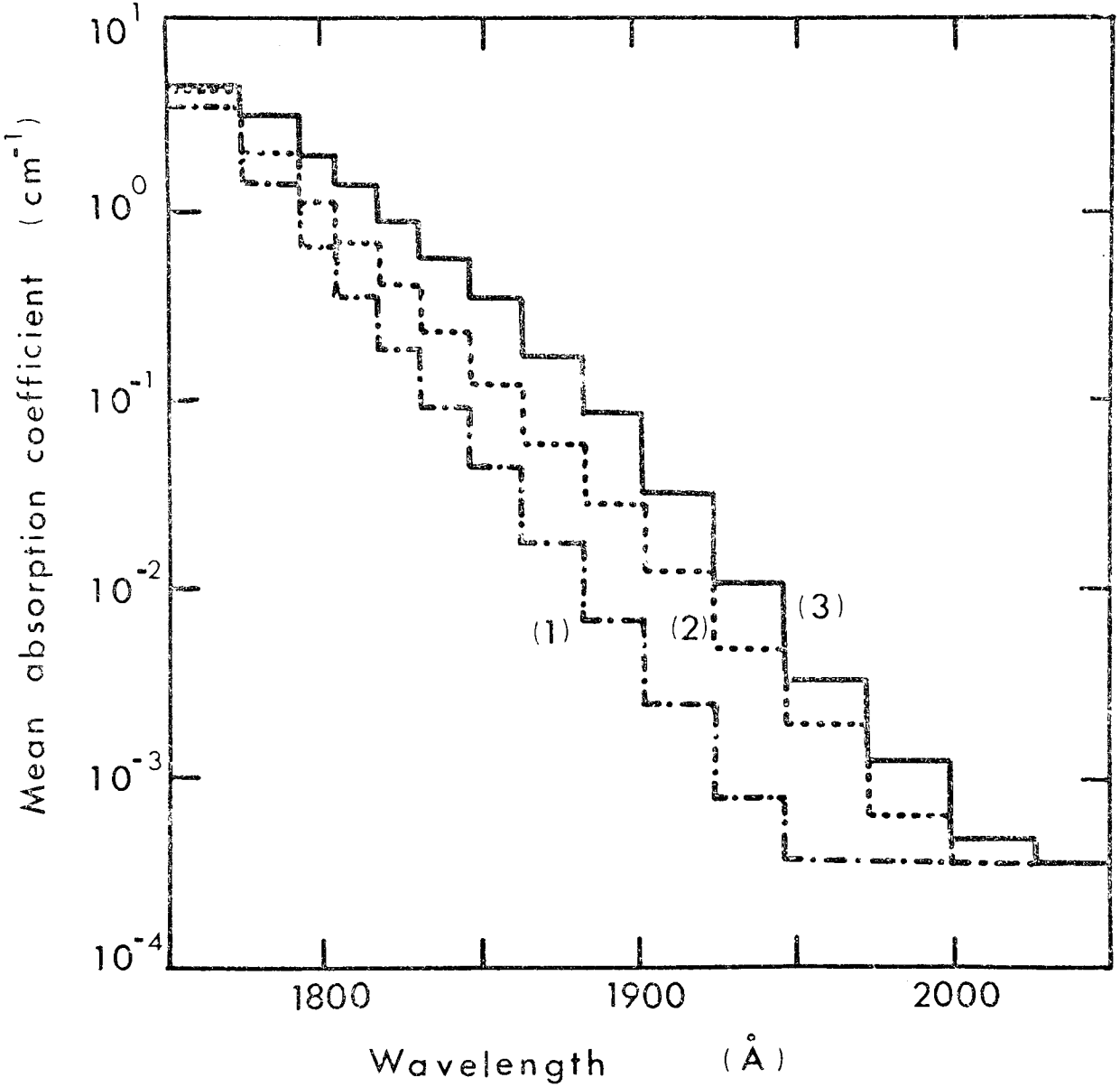
Mean absorption coefficient (cm⁻¹)
10¹
10⁰
10⁻¹
10⁻²
10⁻³
10⁻⁴
1800
1900
2000
Wavelength (Å)
(1)
(2)
(3)

Fig. 19

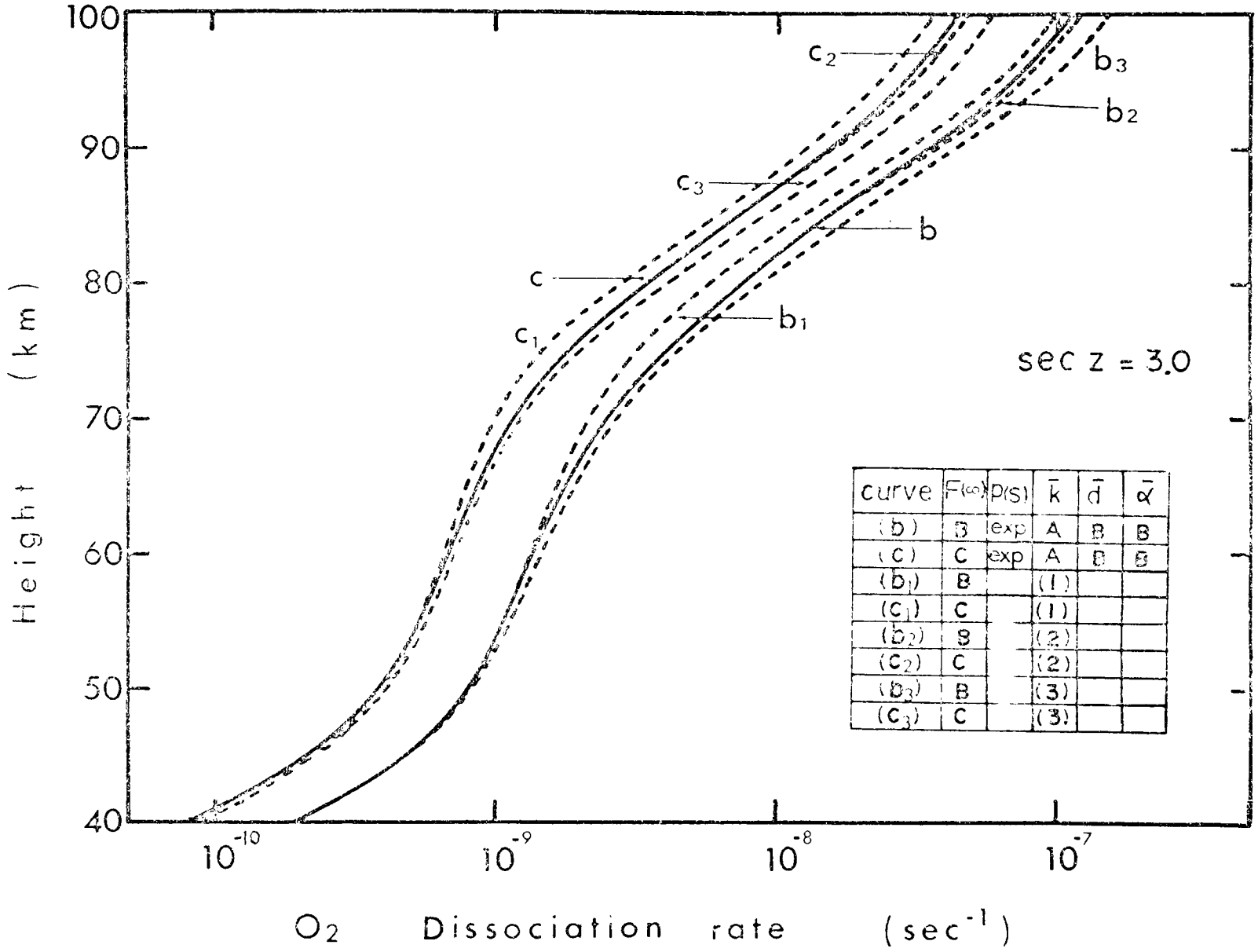
100
90
80
70
60
50
40
Height (km)
10^{-10}
10^{-9}
10^{-8}
10^{-7}
O_2 Dissociation rate (sec^{-1})
c_2
b_3
b_2
c_3
b
c
b_1
c_1
sec z = 3.0
curve | F(ω) | p(s) | k̄ | d̄ | ᾱ
(b) | B | exp | A | B | B
(c) | C | exp | A | B | B
(b_1) | B | | (1) | |
(c_1) | C | | (1) | |
(b_2) | B | | (2) | |
(c_2) | C | | (2) | |
(b_3) | B | | (3) | |
(c_3) | C | | (3) |

Fig. 20

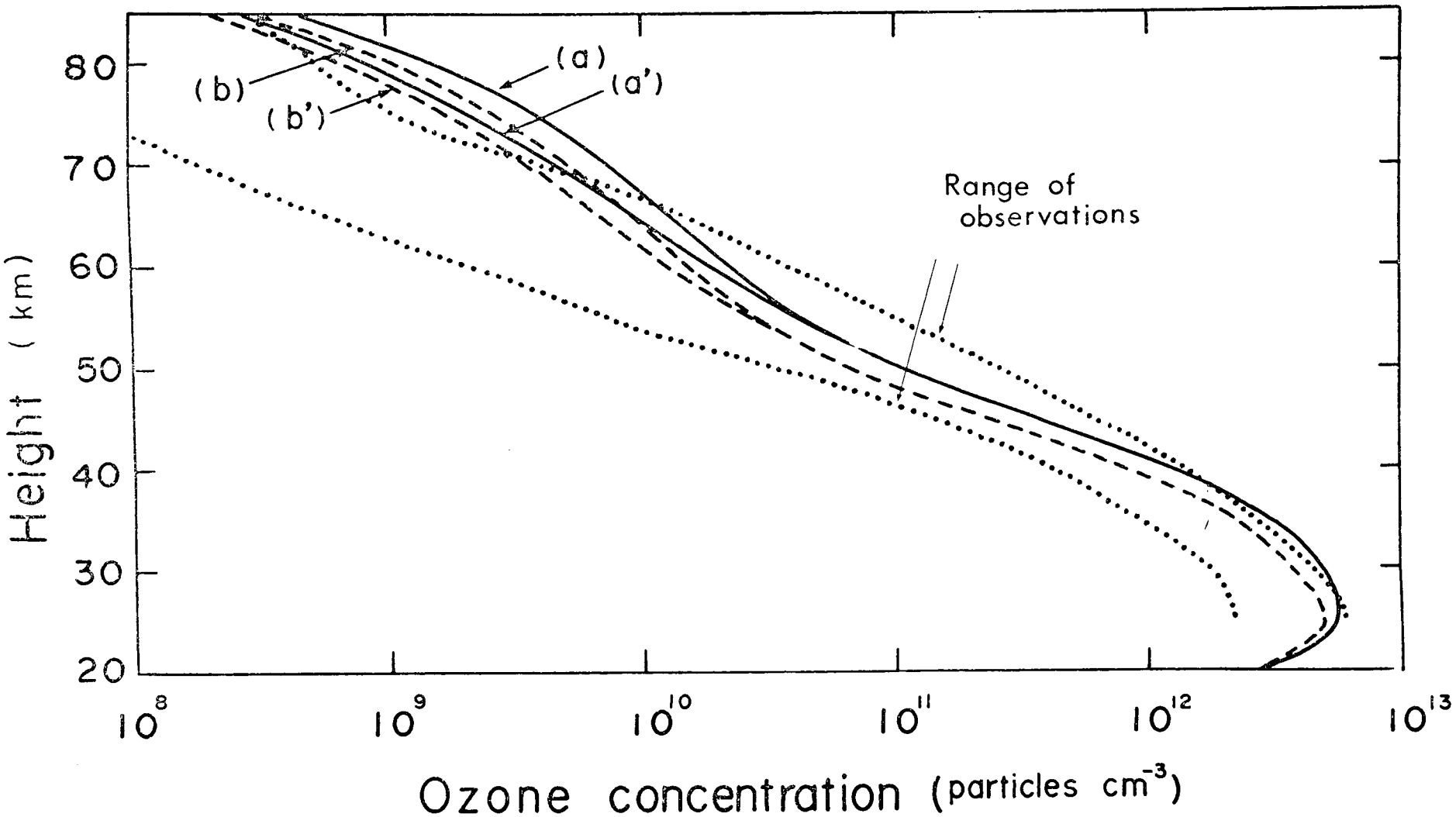
(a)
(a')
(b)
(b')
Range of observations
Height (km)
80
70
60
50
40
30
20
10^8
10^9
10^{10}
10^{11}
10^{12}
10^{13}
Ozone concentration (particles cm^{-3})

Fig. 21

Tables

Table 1

v', v''	$\nu_0(v', 0)$ (cm^{-1})	$\nu_0(v', 1)$ (cm^{-1})	$B_{v'}$ (cm^{-1})	$D_{v'}$ ($10^{-6} cm^{-1}$)	$B_{v''}$ (cm^{-1})	$D_{v''}$ ($10^{-6} cm^{-1}$)
0	49358.15	47801.76	0.8127	5.06	1.437771	4.913
1	50045.68	48489.29	0.8001	6.61	1.421979	4.825
2	50710.83	49154.44	0.7852	5.10	1.406189	4.737
3	51352.26	49795.87	0.7699	4.54		
4	51969.81	50413.42	0.7537	3.56		
5	52561.39	51005.00	0.7372	5.71		
6	53122.79	51566.40	0.7194	5.71		
7	53656.27	52099.88	0.6997	6.96		
8	54156.28	52599.33	0.6771	6.71		
9	54622.17	53065.78	0.6538	7.21		
10	55050.90	53494.51	0.6270	9.75		
11	55438.90	53832.51	0.5980	9.31		
12	55734.57	54228.18	0.5640	14.16		
13	56035.51	54529.12	0.5247	16.8		
14	56340.47	54784.08	0.4836	21.2		
15	56550.54	54994.15	0.4399	25.7		
16	56719.50	55163.11	0.3953	24.3		
17	56852.41	55296.02	0.347	45		
18	56954.54	55398.15	0.296	152		
19	57030.18	55473.79	0.258	49		
20	57082.83	55526.44	0.207	76		

Table 2

v'	Half-width (cm^{-1})	
	Ackerman et al. (1970)	Hudson and Mahle (1972)
0	1.00	0.001
1	1.10	0.002
2	1.20	0.34 ±0.15
3	2.20	1.25 ±0.35
4	3.70	3.30 ±0.20
5	2.30	2.20 ±0.20
6	1.90	1.70 ±0.10
7	2.20	2.25 ±0.05
8	2.00	2.21 ±0.20
9	1.10	0.72 ±0.08
10	1.70	0.34 ±0.05
11	1.70	1.80 ±0.12
12	1.00	0.48 ±0.05
13	0.60	0.08 ±0.05
14	0.50	0.06 ±0.05
15	0.50	0.20 ±0.05
16	0.50	0.25 ±0.05
17	0.50	0.40
18	0.50	0.40
19	0.50	0.40

Table 3

	K(v',0)			K(v',1)
v'	Case A (cm^{-2})	Case B (cm^{-2})	$\frac{K(v',0)_B}{K(v',0)_A}$	Harris et al. (1969) (cm^{-2})
0	9.94 (-3)	9.94 (-3)	1.00	3.53 (-5)
1	9.90 (-2)	9.90 (-2)	1.00	3.20 (-4)
2	5.4 (-1)	6.4 (-1)	1.19	1.81 (-3)
3	1.77 (+0)	3.67 (+0)	2.07	7.09 (-3)
4	6.51 (+0)	1.69 (+1)	2.60	2.08 (-2)
5	1.73 (+1)	6.66 (+1)	3.85	5.02 (-2)
6	4.12 (+1)	1.05 (+2)	2.55	1.05 (-1)
7	8.47 (+1)	1.94 (+2)	2.29	1.97 (-1)
8	1.61 (+2)	2.90 (+2)	1.80	3.29 (-1)
9	2.55 (+2)	3.57 (+2)	1.40	4.90 (-1)
10	3.71 (+2)	4.83 (+2)	1.32	6.67 (-1)
11	5.14 (+2)	6.54 (+2)	1.27	8.37 (-1)
12	6.70 (+2)	8.52 (+2)	1.27	9.65 (-1)
13	7.53 (+2)	8.71 (+2)	1.16	1.03 (+0)
14	7.71 (+2)	8.78 (+2)	1.14	1.03 (+0)
15	7.77 (+2)	8.97 (+2)	1.15	9.59 (-1)
16	7.52 (+2)	7.88 (+2)	1.05	8.50 (-1)
17	6.99 (+2)	7.52 (+2)	1.08	7.09 (-1)
18	5.61 (+2)	4.83 (+2)	0.860	5.66 (-1)
19	4.38 (+2)	4.14 (+2)	0.945	4.35 (-1)
20	2.85 (+2)	3.21 (+2)	1.13	2.82 (-1)

The number in parenthesis is the power of ten of the number in the column.

Table 4

NO	Band Head $v'-v''$	Wavelength Interval ν — ν (cm^{-1})	Mean Line (Half) Half-width $\bar{\alpha}$ (cm^{-1})		Mean Absorption Coefficient[c] $\bar{k}$ (cm^{-2})		Mean Line Spacing $\bar{d}$ (cm^{-1})		
			case A	case B	case A	case B	caseA	caseB	caseC
1	0-0	49358.15 - 48658.15	0.0005	0.166	1.69 (-5)	1.69 (-5)	8.75	8.75	2.92
2	1-0	50045.68 - 49358.15	0.001	0.470	1.55 (-4)	1.55 (-4)	8.81	8.81	2.94
3	2-0	50710.83 - 50045.68	0.17	0.828	8.46 (-4)	1.05 (-3)	9.24	9.24	3.08
4	3-0	51352.26 - 50710.83	0.63	0.939	2.87 (-3)	5.85 (-3)	8.22	8.22	2.74
5	4-0	51969.81 - 51352.26	1.65	1.25	1.08 (-2)	2.78 (-2)	7.92	7.92	2.64
6	5-0	52561.39 - 51969.81	1.10	1.01	3.01 (-2)	1.14 (-1)	7.39	7.39	2.46
7	6-0	53122.79 - 52561.39	0.85	0.699	7.48 (-2)	1.89 (-1)	7.20	7.20	2.40
8	7-0	53656.27 - 53122.79	1.13	0.751	1.61 (-1)	3.65 (-1)	7.02	7.02	2.34
9	8-0	54156.27 - 53656.27	1.10	0.638	3.26 (-1)	5.84 (-1)	6.41	5.56	2.14
10	9-0	54622.17 - 54156.27	0.36	0.228	5.60 (-1)	7.83 (-1)	4.75	2.45	1.58
11	10-0	55050.90 - 54622.17	0.17	0.209	8.98 (-1)	1.19 (+0)	3.97	1.76	1.32
12	11-0	55438.90 - 55050.90	0.90	0.282	1.40 (+0)	1.78 (+0)	2.94	1.15	0.980
13	12-0	55784.57 - 55438.90	0.24	0.159	1.97 (+0)	2.49 (+0)	4.80	1.92	1.60
14	14-0	56340.47 - 55784.57	0.04	0.110	3.05 (+0)	3.48 (+0)	5.67	1.89	1.89
15	20-0	57082.83 - 56340.47	0.17	0.178	4.43 (+0)	4.58 (+0)	6.08	2.03	2.03

[c] The number in parenthesis is the power of ten of the number in the column.

Table 5

Height Km	$N(O_2)$ particles cm^{-2}	$N(O_3)$ particles cm^{-2}
100	1.742 (+18)	1.30 (+13)
95	3.811 (+18)	3.50 (+13)
90	8.749 (+18)	8.82 (+13)
85	2.065 (+19)	2.37 (+14)
80	4.902 (+19)	6.32 (+14)
75	1.128 (+20)	1.55 (+15)
70	2.453 (+20)	3.42 (+15)
65	5.074 (+20)	6.92 (+15)
60	1.004 (+21)	1.36 (+16)
55	1.923 (+21)	2.80 (+16)
50	3.601 (+21)	5.28 (+16)
45	6.738 (+21)	1.46 (+17)
40	1.294 (+22)	4.24 (+17)
35	2.566 (+22)	1.20 (+18)
30	5.273 (+22)	2.82 (+18)
25	1.121 (+23)	5.09 (+18)
20	2.472 (+23)	7.06 (+18)
15	5.642 (+23)	8.30 (+18)
10	1.235 (+24)	9.15 (+18)
5	2.465 (+24)	9.70 (+18)
0	4.556 (+24)	1.01 (+19)

The number in parenthsis is the power of ten of the number in the column.

Table 6

$F_\nu(\infty)$ / Height (km)	Case A Dissociation rate sec^{-1}	Case B Dissociation rate sec^{-1}	Case C Dissociation rate sec^{-1}
secZ = 1.0			
100	0.1008 (-1)	0.1008 (-1)	0.9469 (-2)
95	0.1008 (-1)	0.1007 (-1)	0.9467 (-2)
90	0.1007 (-1)	0.1007 (-1)	0.9463 (-2)
85	0.1006 (-1)	0.1006 (-1)	0.9453 (-2)
80	0.1003 (-1)	0.1003 (-1)	0.9427 (-2)
75	0.9967 (-2)	0.9965 (-2)	0.9367 (-2)
70	0.9840 (-2)	0.9838 (-2)	0.9250 (-2)
65	0.9610 (-2)	0.9608 (-2)	0.9037 (-2)
60	0.9192 (-2)	0.9190 (-2)	0.8650 (-2)
55	0.8370 (-2)	0.8369 (-2)	0.7889 (-2)
50	0.7174 (-2)	0.7173 (-2)	0.6779 (-2)
45	0.4367 (-2)	0.4366 (-2)	0.4163 (-2)
40	0.1878 (-2)	0.1877 (-2)	0.1820 (-2)
secZ = 3.0			
100	0.1008 (-1)	0.1007 (-1)	0.9467 (-2)
95	0.1007 (-1)	0.1007 (-1)	0.9467 (-2)
90	0.1006 (-1)	0.1006 (-1)	0.9451 (-2)
85	0.1003 (-1)	0.1002 (-1)	0.9421 (-2)
80	0.9943 (-2)	0.9943 (-2)	0.9345 (-2)
75	0.9758 (-2)	0.9756 (-2)	0.9174 (-2)
70	0.9398 (-2)	0.9396 (-2)	0.8841 (-2)
65	0.8770 (-2)	0.8769 (-2)	0.8260 (-2)
60	0.7721 (-2)	0.7720 (-2)	0.7287 (-2)
55	0.5987 (-2)	0.5986 (-2)	0.5675 (-2)
50	0.4122 (-2)	0.4121 (-2)	0.3935 (-2)
45	0.1826 (-2)	0.1825 (-2)	0.1773 (-2)
40	0.9015 (-3)	0.9014 (-3)	0.8910 (-3)
secZ = 6.0			
100	0.1007 (-1)	0.1007 (-1)	0.9464 (-2)
95	0.1007 (-1)	0.1006 (-1)	0.9455 (-2)
90	0.1004 (-1)	0.1004 (-1)	0.9433 (-2)
85	0.9976 (-2)	0.9973 (-2)	0.9375 (-2)
80	0.9815 (-2)	0.9813 (-2)	0.9227 (-2)
75	0.9458 (-2)	0.9457 (-2)	0.9897 (-2)
70	0.8784 (-2)	0.8783 (-2)	0.8273 (-2)
65	0.7686 (-2)	0.7685 (-2)	0.7255 (-2)
60	0.6066 (-2)	0.6066 (-2)	0.5750 (-2)
55	0.3951 (-2)	0.3950 (-2)	0.3775 (-2)
50	0.2371 (-2)	0.2371 (-2)	0.2291 (-2)
45	0.1122 (-2)	0.1122 (-2)	0.1104 (-2)
40	0.6358 (-3)	0.6357 (-3)	0.6336 (-3)

The number in parenthesis is the power of ten of the number in the column.